Estuarine, Coastal and Shelf Science 267 (2022) 107766

Contents lists available at ScienceDirect

Estuarine, Coastal and Shelf Science

journal homepage: www.elsevier.com/locate/ecss

Carbon dynamics and CO_2 and CH_4 exchange in the mangrove dominated Guayas river delta, Ecuador

Jean-Philippe Belliard [a,*], Simon Hernandez [a,b,c], Stijn Temmerman [a], Rey Harvey Suello [a], Luis E. Dominguez-Granda [d], Andrea M. Rosado-Moncayo [d], John A. Ramos-Veliz [d], Rebeca N. Parra-Narera [d], Karem Pollete-Ramirez [d], Gerard Govers [e], Alberto V. Borges [f], Steven Bouillon [e]

[a] University of Antwerp, Ecosystem Management Research Group, Antwerp, Belgium
[b] Ghent University, Laboratory of Environmental Toxicology and Aquatic Ecology, Faculty of Bioscience Engineering, Ghent, Belgium
[c] Ghent University, BLUEGent Business Development Center in Aquaculture and Blue Life Sciences, Ghent, Belgium
[d] Escuela Superior Politécnica del Litoral, Centro del Agua y Desarrollo Sustentable, Faculdad de Ciencias Naturales y Matemáticas, Guayaquil, Ecuador
[e] KU Leuven, Department of Earth and Environmental Sciences, Leuven, Belgium
[f] University of Liège, Chemical Oceanography Unit, Liège, Belgium

ARTICLE INFO

Keywords:
Particulate/dissolved carbon
Stable carbon isotopes
Tidal variation
Seasonal variation
Salinity gradient
Guayas river delta

ABSTRACT

Although estuaries are considered important pathways in the global carbon cycle, carbon dynamics in tropical estuaries is relatively understudied. Here, the tidal, seasonal and spatial variability of particulate organic carbon (POC), dissolved inorganic carbon (DIC), carbon dioxide (CO_2) and methane (CH_4), among other biogeochemical variables related to carbon cycling, were studied in the Guayas river delta (Ecuador) to document the sources, processing and fluxes of these carbon forms. All variables were studied during a semi-diurnal (13 h) tidal cycle and along river transects at low and high tides, all carried out during one dry and rainy season. POC and total suspended matter (TSM) strongly covaried and peaked at high tidal flow velocities during a tidal cycle and at high river discharge during the rainy season, suggesting that resuspension of bottom sediments and/or surface erosion in the river catchment were a dominant source of particulate matter in the water column. The $\delta^{13}C$ of POC, (from ~-22‰ to ~-27‰) showed an increasing contribution of marine phytoplankton to the POC pool as moving downstream along the delta during the dry season. Upstream DIC concentrations (~1200 μmol L^{-1}) were high in the Guayas river delta as compared to other tropical estuarine systems, and the $\delta^{13}C$ of DIC revealed a shift from a more phytoplankton dominated source in the dry season and downstream (~-4‰) to a relatively more terrestrial source in the rainy season and upstream (~-12.5‰). Both DIC and its $\delta^{13}C$ showed slight but consistent deviations from conservative mixing that hint at inputs of ^{13}C depleted DIC from mineralization along the delta. High values of the partial pressure of CO_2 (pCO_2) observed upstream and in the rainy season (~5250 μatm), associated with O_2 undersaturation (~60%) and low $\delta^{13}C_{DIC}$, suggest a strongly heterotrophic system, and resulted in high CO_2 efflux to the atmosphere. CH_4 concentrations were also higher during the rainy than dry season (93.5 ± 62.5 vs. 61.3 ± 39.5 nmol L^{-1}), but unlike pCO_2, showed tidal variations similar to TSM and POC, thus alluding to potential CH_4 release from sediments during resuspension events at high tidal flow velocities. This explorative survey revealed complex drivers and biogeochemical processes acting upon various spatio-temporal scales which are necessary to consider for a complete understanding of the carbon biogeochemistry in estuarine systems. Similar surveys on estuarine carbon in data scarce regions are encouraged to constrain uncertainties in coastal zone carbon budgets.

1. Introduction

Situated at the land-ocean interface, estuaries are major pathways of carbon fluxes from the land towards the ocean, and hence play an important role in the global carbon budget. Global estimates show that out of the 12.6 Pg yr^{-1} of terrestrial riverine material discharged to the

* Corresponding author.
E-mail address: jean-philippe.belliard@uantwerpen.be (J.-P. Belliard).

https://doi.org/10.1016/j.ecss.2022.107766
Received 19 July 2021; Received in revised form 23 January 2022; Accepted 31 January 2022
Available online 3 February 2022

world's coastal zones (Beusen et al., 2005; Syvitski et al., 2005), 0.87–1.06 Pg yr^{-1} constitutes of carbon (Li et al., 2017; Ludwig et al., 1996a; Meybeck, 1982; Regnier et al., 2013).

Estuarine carbon is not only limited to terrestrial riverine inputs but may also derive from multiple other sources. Additional allochtonous sources (i.e. externally produced carbon) include marine and anthropogenic inputs (Bala Krishna Prasad and Ramanathan, 2009; Bouillon et al., 2007a; Tue et al., 2012), while autochtonous sources (i.e. locally produced carbon) include estuarine phytoplankton or microphytobenthos, as well as salt marsh and/or mangrove vegetation (Cloern et al., 2014; Couto et al., 2013). These carbon sources vary in their relative importance across estuarine systems, and can be supplied under various forms of carbon, such as particulate and dissolved organic carbon (i.e. POC and DOC) and dissolved inorganic carbon (i.e. DIC). Global riverine export rates of these carbon forms to the coastal ocean have been estimated by various studies in ranges from 0.17 to 0.24 Pg C yr^{-1} for POC (Beusen et al., 2005; Ludwig et al., 1996b; Meybeck, 1982; Mouw et al., 2016; Vitousek et al., 2017), to 0.17–0.25 Pg C yr^{-1} for DOC (Harrison et al., 2005; Li et al., 2019; Liu et al., 2021; Ludwig et al., 1996a; Meybeck, 1982; Vitousek et al., 2017), and 0.32–0.43 Pg C yr^{-1} for DIC (Cai et al., 2008; Li et al., 2017; Ludwig et al., 1996a; Meybeck, 1982). The dominance of the export of DIC over DOC and POC has been consistently found across recent case studies (e.g. Huang et al., 2012; Regnier et al., 2013; Sadat-Noori et al., 2016).

All three forms of carbon are linked to each other via biogeochemical processes (such as respiration, photosynthesis, calcification) and mixing processes. The sources and processing rates of estuarine carbon can vary over various time and spatial scales within an estuary. For instance, studies have shown that changes in tidal levels (e.g. Barboza et al., 2014, Bouillon et al., 2007b,c), seasonal changes associated with river discharge (e.g. Guo et al., 2015; Hoffman and Bronk, 2006), and the distribution and mixing of different water masses along the salinity gradient (e.g. Bouillon et al., 2003) all influence the sources, concentrations and fluxes of POC, DOC and DIC.

Coastal wetlands such as salt marshes and mangroves, which are intrinsic to estuaries and deltas, also play an important role in carbon dynamics. Mangroves, in particular, are among the most productive coastal ecosystems on Earth (Alongi, 2014; Donato et al., 2011), with global net primary production of about 200 Tg C yr^{-1} (Alongi and Mukhopadhyay, 2015; Bouillon et al., 2008). Furthermore, above- and belowground organic carbon stocks per unit surface area in mangroves are among the highest reported for any ecosystem type, making them important carbon sinks (Alongi, 2014; Atwood et al., 2017; Bouillon et al., 2008; Ouyang and Lee, 2020; Rovai et al., 2018). Yet, the majority of the mangrove derived carbon is tidally exported to the ocean as POC, DOC and DIC via porewater or tidal surface water exchange with adjacent tidal creeks and estuarine channels (Maher et al., 2013, 2018; Sippo et al., 2016; Taillardat et al., 2018), or is directly exchanged as carbon dioxide (CO_2) and methane (CH_4) through remineralization of organic matter (Rosentreter et al., 2018a; 2018b).

Organic and inorganic carbon therefore undergo profound transformations in estuaries, which often results in strong heterotrophic systems, i.e. where respiration rates exceed local primary production (Borges and Abril, 2012; Caffrey, 2004; Gattuso et al., 1998). As a consequence, most estuaries worldwide are oversaturated with dissolved CO_2 and CH_4 and are known to be a significant source of these greenhouse gases to the atmosphere on regional and global scales (Borges and Abril, 2012; Rosentreter et al., 2021). Estuaries thus represent a biogeochemically active zone, and given their importance in the global carbon cyle and budget (Bauer et al., 2013; Borges, 2005; Cole et al., 2007; Regnier et al., 2013), understanding the sources, processing and fate of the different carbon forms across a variety of estuarine systems is essential.

Studies on the biogeochemistry of carbon in tropical estuaries are rather limited in comparison to temperate estuaries, despite ~60% of the global riverine carbon flux being estimated to take place in the tropics (Ludwig et al., 1996a,b). Especially, the South American tropical region remains largely understudied, with the few detailed studies on carbon cycling almost all focusing on Brazilian estuaries (see Borges and Abril, 2012), while to the best of our knowledge, no similar studies exist for South American tropical estuaries bordering the Pacifc ocean. Among the South American rivers discharging into the Pacific ocean, the Guayas river delta (Ecuador) is the largest estuarine system and drains the largest tropical river basin in the region (Cifuentes et al., 1996). Yet, the biogeochemistry of the Guayas river delta has received little attention so far. One study addressing the isotopic and elemental variations of carbon and nitrogen in suspended particulate matter suggested that organic matter is mainly derived from riverine material and detritus from mangroves (Cifuentes et al., 1996). Another study focusing on litter dynamics of the mangroves in the Guayas river delta showed that the fate of leaf litter is dependent on the relative effects of geophysical (tides and river discharge) and ecological (crab activity) processes (Twilley et al., 1997). Most studies have rather focused on the water quality and biology in the freshwater part of the Guayas river basin (Borbor-Cordova et al., 2006; Damanik-Ambarita et al., 2018; Deknock et al., 2019), but a lack of knoweldge remains on the carbon biogeochemistry in the estuarine zone (i.e. with tides and salinity gradient) of the delta.

Here, we investigate the sources, processing and fate of different forms of carbon in the Guayas river delta, and how these vary during tidal cycles, along the land-to-sea (salinity) gradient, and between seasons.

2. Materials and methods

2.1. Study area

The Guayas river, the most important of Ecuador with regard to its catchment area (~32,000 km^2; Borbor-Cordova et al., 2006) and more so for its economic significance, begins at the confluence of the Babohoyo and Daule rivers and runs over 70 km to the south before flowing into the Gulf of Guayaquil that is connected to the Pacific ocean (Fig. 1). Along its course, the Guayas river forms a large delta which, together with the Gulf of Guayaquil, constitutes the largest estuarine system on the Pacific coast of South America (Twilley et al., 2001).

The Guayas river delta (2°00′S–3°00′S and 80°15′W–79°45′W) is characterized by multiple branches of river channels and tidal creeks which intersect a large deltaic floodplain covered by dense mangrove forests (dominated by *Avicennia germinans* and *Rhizophora somoensis*) and tidal flats, totalling an area of ca. 4000 km^2. The Churute reserve alone, situated east of the delta, covers and protects 12,000 ha of mangroves. Tides are semi-diurnal and the mean tidal range increases from approximately 2 m at the downstream end of the delta (near the Island of Puná and km zero, see Fig. 1) to around 4 m at around 60 km upstream at Guayaquil (Fig. 2a), making the Guayas river delta a tide dominated delta. Tidal range decreases further upstream and attenuates at around 90 and 120 km in the Babahoyo and Daule rivers, respectively. The climate is equatorial, driven by the annual migration of the intertropical convergence zone that produces a dry season (December to May) followed by a rainy season (June to November) when 95% of annual precipitation occurs. As a result, the freshwater discharge in the Guayas river has a strong seasonal variability (Fig. 2b), ranging from 200 $m^3 s^{-1}$ during the dry season to 1600 $m^3 s^{-1}$ during the rainy season for a year of average precipitation (about 900 mm yr^{-1}; INOCAR, 2019). As such, the Guayas river delta becomes increasingly river dominated in the rainy season. Discharge and tides in the Guayas river delta also show an interannual variability driven by the El Niño–Southern Oscillation, which can produce record extreme sea levels coinciding with extreme precipitation and river discharge, hence producing risks for exceptional flooding of inhabited regions of the delta during strong El Niño events (Belliard et al., 2021). Due to the strong tidal and riverine influences, and water depths not exceeding 10 m, the Guayas river delta is classified as a vertically well-mixed estuary (Twilley et al., 2001).

Fig. 1. The Guayas river delta (Ecuador) with the location of the sampling sites along a river transect and two tidal side channels (i.e. S1 and S2) where spatial sampling campaigns were conducted, and a site in front of the village of Puerto Roma where temporal sampling campaigns were conducted.

The Guayas river and its delta are extremely important to the economy of Ecuador. The river catchment concentrates most of the national agricultural, industrial and manufacturing production (Borbor-Cordova et al., 2006). The delta alone is home to ca. 3.1 million people, most of which live in the city of Guayaquil, Ecuador's largest population and economic centre. Yet, human settlements and resulting anthropogenic activities in the Guayas river delta have caused great pressure on the surrounding environment. Guayaquil, which sits right on the Guayas river in the northern part of the delta, has been gradually expanding into former mangrove forests. Mangrove loss in the delta has also been associated with shrimp aquaculture (see Fig. 1) that started in the 1960s and which nowadays provides an annual economic profit of ca. US$ 3.1 million (ICEX, 2019). During the period 1984–2014, an estimated 22,000 ha of mangrove forests were converted into shrimp farms and today about 112,100 ha of mangrove forests remain (Hamlington et al., 2016). In addition to land use changes, the Guayas river delta has also seen changes in water quality caused by the input of nutrients and pesticides from agriculture and aquaculture, sewage from large urban areas such as Guayaquil and Durán, and heavy metals from industry (Twilley et al., 1998). All these anthropogenic activities are therefore likely to influence the ecology and biogeochemistry of the delta.

2.2. Sampling campaigns

Field sampling was carried out during two 3-week campaigns, one during the dry season (September 2018) and another during the rainy season (March 2019). During each campaign, we measured (i) temporal variations in a series of aquatic biogeochemical parameters during a semi-diurnal tidal cycle at one location in the delta, and (ii) spatial variations in these biogeochemical parameters along the deltaic land-to-sea gradient.

First, for the temporal variations, we sampled from a boat anchored at one site in the middle of the main channel of the Guayas river, in front

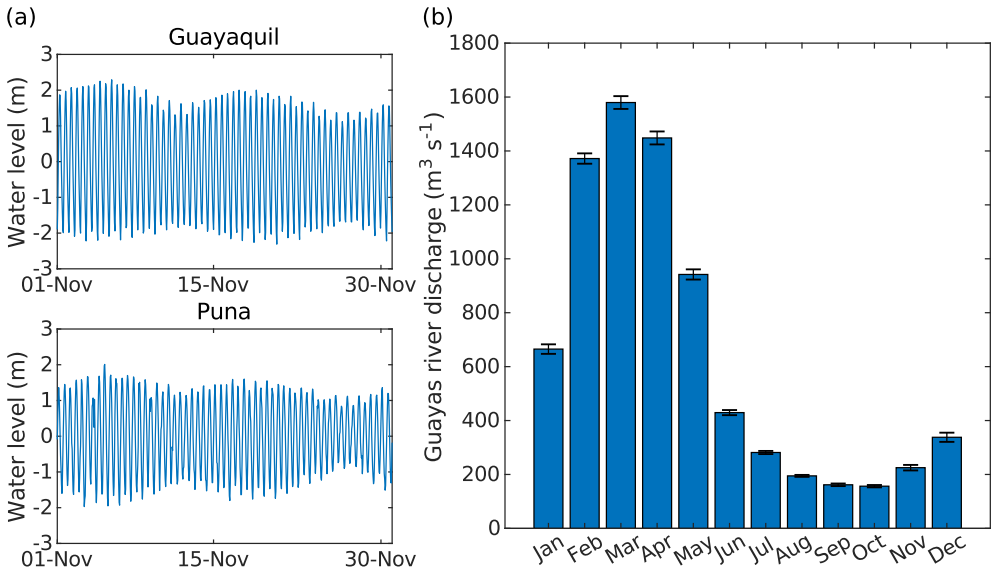

Fig. 2. (a) Water levels in November 2013 recorded by the tide gauge stations of Puná (near the downstream end of the Guayas river delta) and Guayaquil (about 60 km upstream; see locations in Fig. 1). Data acquired from INOCAR (Ecuadorian Oceanographic National Institute). (b) Monthly average discharge for the Guayas river. The discharge was calculated by summing up discharge records during the period 1984–2015 from several river gauge stations located along the Babahoyo and Daule tributaries. Error bars represent ±1 SE. Data acquired from INHAMI (Ecuadorian Meteorological and Hydrological National Institute).

of the village of Puerto Roma (2°30′53′′S, 79°52′58′′W; see Fig. 1). Sampling and direct insitu measurements were performed every 30 min for 13 h in order to cover a complete semi-diurnal tidal cycle. We recognise that ideally a 25 h measuring campaign allows to capture potential day and night cycles in the measured variables. However, because of practical and logistical constraints, we conducted our temporal sampling only during daylight time for 13 h. This sampling is still appropriate to capture variability over a single semi-diurnal tidal cycle, as here in the Guayas river delta, tides do not exhibit a significant diurnal inequality, and rather show a clear and consistent semi-diurnal tidal pattern (Zapata et al., 2019). These characteristics result in minimal changes in tidal amplitudes and phases between successive tides, provided similar meteorological conditions. This sampling was carried out on September 25th (dry season) and March 19th (rainy season).

Second, for the spatial variations, during each campaign we carried out sampling at several sites along the length of the delta both at low and high tides. This was done by cruising with a motored boat from the most downstream to upstream sampling sites, following the upstream propagation of the low and high stages of the tidal wave. As such, all sites were consistently sampled at the time of low and high tides, respectively. The sampling sites were distributed every 5 km along a transect starting offshore from Punta Mandinga on the island of Puná (site 0 km), which more or less marks the mouth of the Guayas river, and ending at the island of Santay (site 60 km), in order to cover a salinity gradient as large as possible (see Fig. 1). This river transect was also defined by selecting a course that bordered large areas of mangrove forests, including the Churute reserve, in order to capture the influence of the mangroves on the sources, processing and fluxes of the studied carbon forms. However, for practical, logistic and safety reasons, we had to conduct the temporal sampling in another estuarine channel (see Fig. 1). Two sampling cruises were necessary per tidal stage to be able to sample the river transect every 5 km while keeping pace with the upstream propagation of the low and high tides. Specifically, for each of the two low tide (and high tide) cruises, samples and insitu measurements were carried out every 10 km over the full length of the transect, with the first cruise starting from site 0 km and the second from site 5 km, to eventually recover the 5 km spatial resolution. Both low tide cruises were carried out on consecutive days (September 11th and 12th in the dry season and March 7th and 8th in the rainy season), as were the high tide cruises one week later to wait for feasible tidal timing (September 18th and 19th in the dry season and March 14th and 16th in the rainy season).

During the various sampling cruises along the river transect, we additionally sampled at two sites in the two tidal side channels, situated within the Churute reserve, which drains directly into the Guayas river branch at low tide where the transect was established (see Fig. 1). As such, these sites are representative of a mangrove influenced water source. and sampling there allows to capture the spatial complexity of the delta and contribute to a more comprehensive understanding of the carbon inputs, sources and processing in the delta.

2.3. Sample collection and analytical techniques

For all sampling sites, both insitu measurements and water sampling were carried out. Physico-chemical parameters (dissolved oxygen (DO) and oxygen saturation level (%O_2), pH, temperature, conductivity and salinity) were directly measured from the boat just below the water surface using a water quality portable mutlimeter (HQ40d, HACH), which consisted of a DO and temperature probe (Intellical LDO101) with an accuracy of ±0.1 mg L^{-1} and ±0.3 °C, respectively; a pH probe (Intellical PHC101) with an accuracy of ±0.02; and a salinity probe (Intellical CDC401) with an accuracy of ±0.1. Water depth was measured using a high frequency digital depth sounder (Hondex, Jeetekno) as well as a portable CTD (CastAway-CTD, SonTek) with an accuracy of ±1% and ±0.25%, respectively.

A 3L Niskin bottle was used to sample surface water at ~0.5 m below the surface. Water samples needed for later lab filtration were directly stored into two 1 L opaque plastic bottles which were placed inside a cool box. Samples for the determination of total suspended matter (TSM) were obtained by filtering a large volume of surface water through pre-weighted and pre-combusted 47 mm diameter filters (Whatmann GF/F 0.7 μm pore size) until almost clogged while documenting the filtered volume. Filters were then dried at 50 °C at least overnight. The weights before and after filtration, and the corresponding filtered water volume were used to calculate TSM concentration. Samples for determination of total alkalinity (TA) were prepared by passing a volume of filtered water from the TSM filtration through 0.2 μm Acrodisc syringe filters. Resulting samples were subsequently stored in HDPE bottles until analysis by automated electro-titration with a Metrohm titrator using 0.1 M HCl as titrant, with a reproducibility of 3 μmol L^{-1}.

Samples for the determination of POC, its contribution to TSM (POC: TSM ratio, expressed as a %), and $\delta^{13}C$ of POC ($\delta^{13}C_{POC}$) were obtained by filtering surface water through pre-combusted 25 mm diameter filters (Whatmann GF/F 0.7 μm pore size). Filters were then exposed to HCl fumes for 4 h to remove carbonates, and dried at 50 °C at least overnight. Hereafter, filters were encapsulated in silver cups and stored in well plates until analysis. The stable isotope ratio $\delta^{13}C$ (reported in permil,

‰) for POC (and DIC) is expressed as:

$$\delta^{13}C = \left(\frac{R_{sample}}{R_{standard}} - 1\right) * 1,000 \quad (1)$$

where R_{sample} and $R_{standard}$ are the isotopic ratios $^{13}C/^{12}C$ of the sample and V-PDB (Vienna Pee Dee Belemnite), respectively. POC and particulate nitrogen (PN) concentrations as well as their ratios (POC:PN, expressed in weight/weight), and calibration of the $\delta^{13}C$ of POC ($\delta^{13}C_{POC}$) were determined on an EA-IRMS (Thermo FlashHT with DeltaV Advantage) elemental analyzer–isotope ratio mass spectrometer in combination with different certified (IAEA-600, i.e. caffeine) and in-house (Leucine, Tuna) standard materials. Reproducibility of $\delta^{13}C_{POC}$ measurements was generally better than ±0.1‰.

Samples for the determination of $\delta^{13}C$ of DIC ($\delta^{13}C_{DIC}$) and CH_4 were taken directly from the Niskin bottle. For $\delta^{13}C_{DIC}$, 12 mL Exetainer vials (Labco) were gently overfilled, poisoned with 20 μL of a saturated $HgCl_2$ solution, and sealed with a cap containing a butyl rubber plug. Before the analysis, a He headspace was created and ±10 drops of saturated H_3PO_4 was added to convert inorganic carbon species (HCO_3^- and CO_3^{2-}) into CO_2. After overnight equilibration, part of the headspace was injected into the He stream of the EA-IRMS to eventually determine $\delta^{13}C_{DIC}$ (reproducibility was ±0.05‰). For CH_4, 60 mL borosilicate serum bottles (Wheaton) were overfilled, poisoned with 50 μL saturated $HgCl_2$ solution, and sealed gas-tight with a butyl rubber stopper and aluminum cap. Samples were stored at room temperature until analysis. Before analysis, a N_2 headspace was created, samples were vortexed, placed on a benchtop shaker for 20 min, and allowed to equilibrate overnight. The following day, part of the headspace was injected into a gas chromatograph (GC, SRI 8610C) with a flame ionization detector for CH_4 (reproducibility was ±2 nmol L^{-1}), calibrated with gas standards from Air Liquide Belgium of 1, 10 and 30 ppmv CH_4.

To measure the partial pressure of CO_2 (pCO_2), three 60 mL syringes fitted with 3-way valves were filled with surface water, while avoiding air bubbles in the syringes. Water was then expelled from these syringes until only 30 mL of water remained. Hereafter, 30 mL of ambient air was sucked into the syringes to create a headspace, resulting in equal volume of 30 mL headspace and 30 mL water. A fourth syringe was filled completely with ambient air. Filling of the syringes with air was done simultaneously to ensure that the same air was used. Syringes were shaken for 10 min to equilibrate, after which pCO_2 of air and of the headspace inside each syringe was measured in the field using a CO_2 gas analyzer (LI-820, LI-COR), and water temperature inside each syringe was measured with a digital thermometer (HI 147–00, Hanna instruments) in September 2018 and a temperature sensor (Arduino DS18B20) in March 2019. The pCO_2 and DIC of the surface water were then calculated from the measured pCO_2 in equilibrated air, TA and water temperature, following the method by Lewis and Wallace (1998). The pCO_2 and DIC values were computed with an accuracy of ±2.0% and ±5 μmol L^{-1}, respectively. Note that DOC concentrations were not determined here because of the limitation of the associated lab analyzing equipment for samples in brackish/saline conditions.

2.4. Mixing models

To understand the behaviour of DIC and $\delta^{13}C_{DIC}$ along the salinity gradient, a mixing model was applied using salinity as a conservative tracer. The conservative mixing model for DIC was calculated using the following equation:

$$DIC = \frac{DIC_M - DIC_F}{S_M - S_F} * S + DIC_M - \frac{DIC_M - DIC_F}{S_M - S_F} * S_M \quad (2)$$

where DIC is the calculated value for salinity S, DIC_M and DIC_F are the DIC concentrations of the marine end-member (i.e. the highest salinity data point) and freshwater end-member (i.e. the lowest salinity data point), respectively. Similarly, S_M and S_F are the salinity of the marine and freshwater end-members, respectively.

For $\delta^{13}C_{DIC}$, the conservative mixing model was calculated following Mook and Tan (1991):

$$\delta^{13}C_{DIC} = \frac{S*(DIC_F*\delta^{13}C_F - DIC_M*\delta^{13}C_M) + S_F*DIC_M*\delta^{13}C_M - S_M*DIC_F*\delta^{13}C_F}{S*(DIC_F - DIC_M) + S_F*DIC_M - S_M*DIC_F} \quad (3)$$

where $\delta^{13}C_{DIC}$ is the calculated value for salinity S, and $\delta^{13}C_F$ and $\delta^{13}C_M$ are the $\delta^{13}C$ values of the freshwater and marine end-members, respectively.

2.5. Calculation of estimated carbon diffusive fluxes

The diffusive exchange flux of greenhouse gases across the air-water interface was calculated according to: $F = \varepsilon*k*\alpha*\Delta gas$, where ε is the chemical enhancement factor of gas exchange, k is the gas transfer velocity of the respective gas, α is the solubility coefficient of CO_2 (Weiss 1974) or CH_4 (Yamamoto et al., 1976), and Δgas is the difference in partial pressure of the respective gas of air and water. k in estuarine settings is known to vary depending on a number of site-specific environmental factors including wind speed, water currents, fetch limitation, among others. Here, to calculate CO_2 fluxes, we estimated the value of k following its parametrization by Borges et al. (2004) for the Scheldt and Thames estuaries, two other examples of macrotidal systems as the Guayas river delta. To calculate CH_4 fluxes, we followed the k parametrization by Raymond and Cole (2001). Because no wind speed measurements were taken here, we used an average wind speed value at the Puná and Guayaquil tide gauge stations provided by INOCAR.

We determined the export rate of any form of carbon E_c based on the simple equation: $E_c = C_F*Q$, where C_F is the carbon form concentration at the freshwater end-member and Q is the Guayas river discharge (with a daily average value between 559 and 783 $m^3\ s^{-1}$). The freshwater end-member is defined as the upstream sampling sites located in the main channel (km 45–60; see Fig. 1) where we averaged all local concentration values measured over the various river cruises conducted at low tide. Discharge for the Guayas river was calculated by summing up daily discharge records during the period 1982–2015 from several river gauge stations located along the Babahoyo and Daule tributaries. These resulting daily discharge data were then averaged per season and year over the entire measurement period, from which minimum, mean and maximum seasonal and annual river discharge were computed. Note that we make here the assumptions that (i) all carbon that was transported at our freshwater end-member sites either remained unchanged, or was partially lost and replenished again, as it was transported along the land-to-sea gradient, (ii) the discharge measured upstream of the Guayas river delta was equal to the discharge at the estuary mouth. We therefore acknowledge ahead that these export rates represent approximate estimations.

2.6. Statistical analyses

Means of the various investigated variables were compared using

unpaired t-tests (Table S1). If the data were not normally distributed, a log- or reciprocal-transformation was applied to the data in an attempt to attain normality. In parallel, a non-parametric Wilcoxon rank sum test was also performed. Correlation between paired variables were assessed using Pearson product moment correlation r coefficient or Spearman's rank correlation coefficient ρ when the data were not normally distributed (Tables S2–S4). All statistical methods were carried out with a 95% confidence interval.

3. Results

3.1. Tidal and seasonal variations

3.1.1. Physico-chemical parameters

Salinity values ranged from 11 at low tide to 23 at high tide, during the semi-diurnal tide sampled in the dry season at the sampling site in front of Puerto Roma (see Fig. 1). Comparatively, values only varied from 0 at low tide to only 2 at high tide during the rainy season (Fig. 3a–b). This reveals a strong seasonal salinity shift in the system. Salinity changes over the semi-diurnal tidal cycle co-varied well with the changes in water levels in the dry season, while in the rainy season the salinity remained constantly low around periods of low tide, before increasing slightly midway during the flood tide. Also, temperature and pH showed a stronger response to tidal water level variations in the dry season (Supplementary Information Figs. S1a–b and Figs. S1c–d), with maxima occurring at low and high water slacks, respectively. DO and % O_2 remained relatively constant during the tidal cycle, but showed a temporary increase during the rising tide in both rainy and dry seasons (Figs. S1e–f and Figs. S1g–h). Values were systematically higher in the dry than rainy season.

3.1.2. Concentrations and characteristics of suspended particulate matter

In the dry season, we observe TSM concentrations varying from as low as 30 mg L^{-1} to above 350 mg L^{-1}. TSM values generally remained below 100 mg L^{-1}, but higher peaks occurred around mid ebb and flood tides (Fig. 4a), and minima occurred shortly after low and high tides. In the rainy season, TSM was characterized by higher values ranging from 60 to 280 mg L^{-1} (Fig. 4b). In contrast to the dry season, TSM concentrations remained relatively high and constant around low tide. POC patterns strongly resembled those of TSM in both seasons (Fig. 4c–d), although with some deviations around low tide in the rainy season. POC concentration varied from 1 to 5 mg L^{-1} both in the dry and rainy seasons. Except for a sudden peak during ebb tide, POC:TSM ratios remained constant in the dry season, but showed some fluctuations in the rainy season (Fig. 4e–f). POC:TSM values were significantly higher in the rainy than dry season (Wilcoxon rank sum test: $Z = -2.90$, $p < 0.05$). Tidal variation in POC:PN ratios increased from the dry to rainy season, with values fluctuating around 6–10 and 7–14, respectively (Fig. 4g–h). The pattern of variation of POC:PN ratios in the dry season largely followed patterns of TSM and POC, where high POC:PN values coincided with high TSM and POC values. Correlations between the respective variables however slightly weakened in the rainy season ($\rho = 0.68$ vs. $\rho = 0.80$ for POC:PN tested against POC; $\rho = 0.57$ vs. $\rho = 0.77$ for POC:PN tested against TSM, both significant at $p < 0.05$). $\delta^{13}C_{POC}$ showed a tidal variation that was different from POC and POC:PN ratios, particularly in the dry season, where $\delta^{13}C_{POC}$ co-varied with water levels. $\delta^{13}C_{POC}$ values ranged from −26‰ to −24‰ in the dry season and from −26.5‰ to −25‰ in the rainy season (Fig. 4i–j).

3.1.3. Dissolved inorganic carbon and methane dynamics

A seasonal shift, similar to salinity, also characterized the tidal variation of DIC concentrations. Values ranged from about 1700 µmol L^{-1} at low tide to 2030 µmol L^{-1} at high tide in the dry season, whereas maximum values at high tide never exceeded 1200 µmol L^{-1} in the rainy season (Fig. 5a–b). DIC followed the patterns of salinity more closely in the dry than rainy season (see Fig. 3a–b). Tidal variation of $\delta^{13}C_{DIC}$ depicted a similar seasonal pattern as DIC and salinity. Specifically, values varied from less than −8‰ at low tide to nearly −4‰ at high tide in the dry season, and from −13‰ at low tide to about −12‰ at high tide in the rainy season (Fig. 5c–d). Also here, $\delta^{13}C_{DIC}$ pattern agreed better with those of DIC and salinity in the dry than rainy season.

pCO_2 showed a significant increase from dry to rainy season (Wilcoxon rank sum test: $Z = -6.30$, $p < 0.001$). Values ranged between 1200 and 2200 µatm in the dry season and between 4000 and 5100 µatm in the rainy season, respectively (Fig. 5e–f). Note that patterns of relative pCO_2 variations over the semi-diurnal tide cycles were similar between the two seasons, with maxima occurring at low tide and minima at high tide. During the dry season, CH_4 concentrations ranged from 40 to 130 nmol L^{-1}, while during the rainy season, values ranged from 28 to 115 nmol L^{-1}, with a few peaks above 200 nmol L^{-1}. Regardless of the season, CH_4 maxima occurred at mid flood and ebb tides, whereas CH_4 minima occurred at low and high water slacks (Fig. 5g–h). This pattern resembles those of particulate carbon forms previously described (see Fig. 4), particularly in the dry season ($\rho = 0.60$, $\rho = 0.59$ and $\rho = 0.46$ when tested against TSM, POC and POC:PN ratios, respectively).

3.2. Spatial and seasonal variations

3.2.1. Physico-chemical parameters

During the transect sampling, the salinity gradient along the river showed a strong seasonal shift for both low and high tides (Fig. 6a–b), which is consistent with the above-observed semi-diurnal tidal variations in salinity (see Fig. 3). In the dry season, values ranged from about 5 at the upstream end of the river transect to almost 25 at the downstream end, thus depicting a strong gradient covering oligohaline regions upstream to mesohaline and polysaline regions midstream and downstream, respectively (Fig. 6a). This gradient was much weaker in the rainy season, characterized by salinity values varying from 0 already half way the sampled river transect to less than 10 at the actual downstream end of the river transect (Fig. 6b). Temperature and pH remained

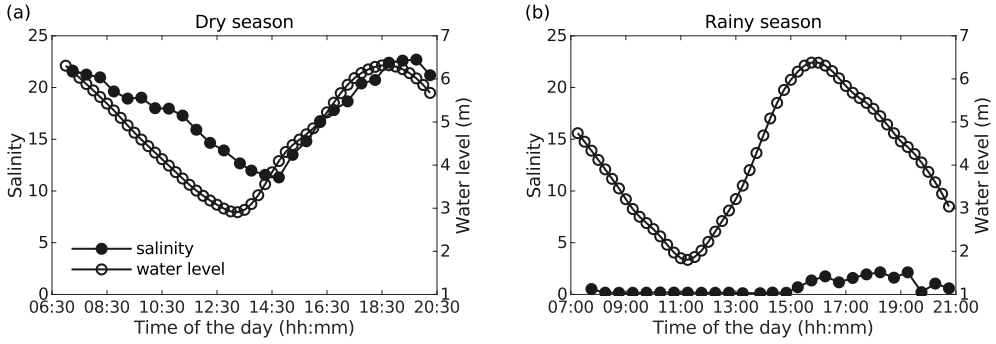

Fig. 3. Tidal variations of water levels and salinity in the (a) dry and (b) rainy seasons, resulting from the sampling campaigns during semi-diurnal tidal cycles in the Guayas main channel in front of Puerto Roma (see location in Fig. 1).

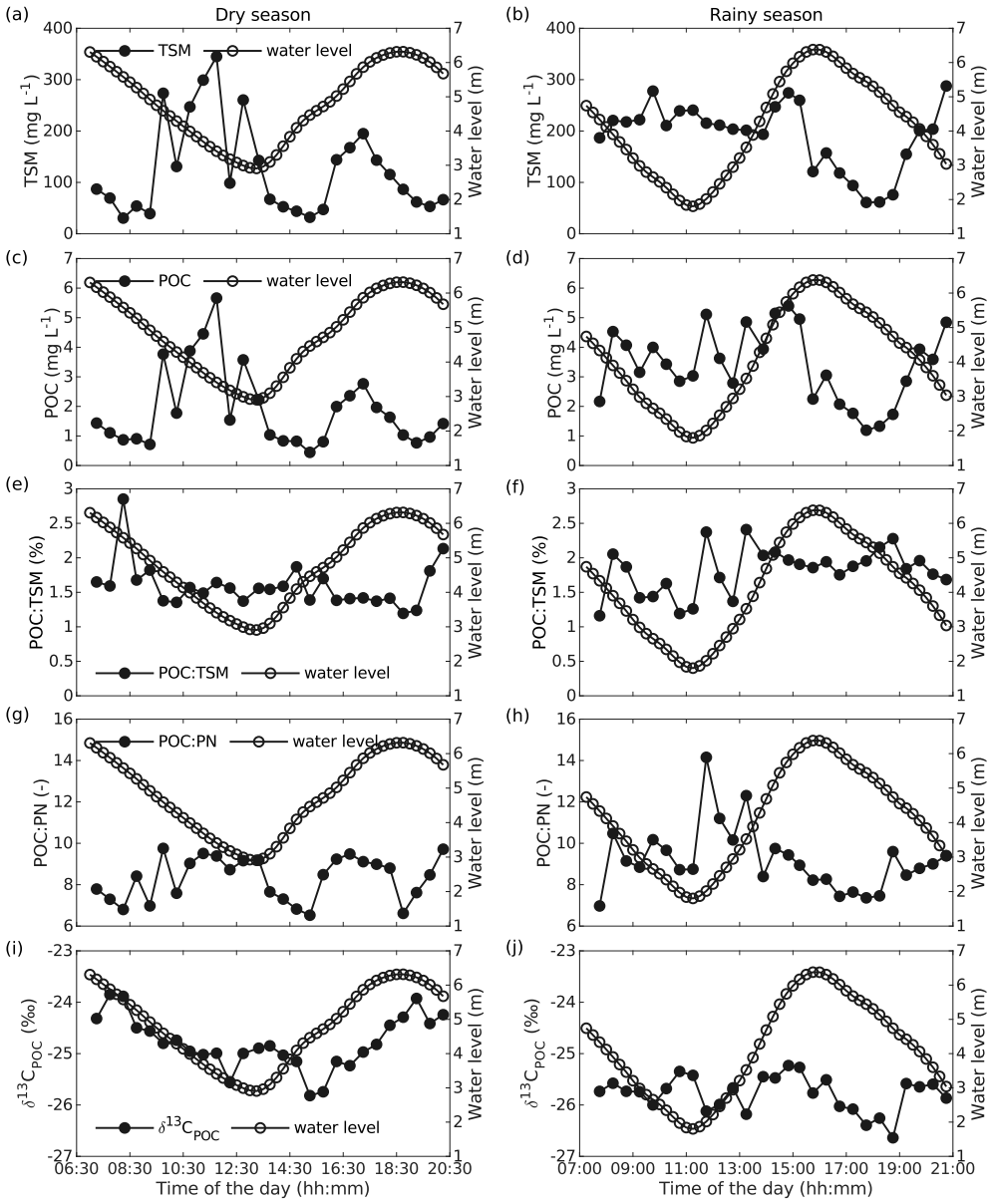

Fig. 4. Tidal variations of water levels and (a,b) TSM, (c,d) POC, (e,f) POC:TSM, (g,h) POC:PN and (i,j) $\delta^{13}C_{POC}$ in the dry (left panels) and rainy season (right panels). Data resulted from the sampling campaigns during the semi-diurnal tidal cycles in the Guayas main channel in front of the village of Puerto Roma (see location in Fig. 1).

relatively constant along the river length in both seaons and tidal stages, although there was a sharp local drop in pH downstream of the river transect during the high tide sampling cruise in the rainy season (Figs. S4a–d). Conversely, we observed overall a gradual increase in % O_2 level and DO upstream during the rainy season, which was particularly pronounced during the low tide cruises, while these parameters remained relatively constant along the river transect during the dry season (Figs. S4e–h).

3.2.2. *Concentrations and characteristics of suspended particulate matter*

When plotted against salinity, and considering all measurements (i.e. including the sampling during the semi-diurnal tidal cycles, along the river transect, and in side channels), POC showed no clear nor distinctive patterns between tidal stages and seasons (Fig. 7a). This lack of trend is also manifested by large differences in POC values between similar individual river transects (i.e. at same tidal stage and season) that were conducted on consecutive days, although this is particularly pronounced for the river transects at low tide (Figs. S2a–b). POC showed a weak negative correlation with salinity ($\rho = -0.51$; $p < 0.05$) which corroborates the spatial variation of POC along the river transect that showed at high tide a gradual decrease downstream in both seasons (Figs. S2a–b and Figs. S5c–d). POC:TSM ratios did not depict any pattern with salinity (Fig. 7b), as also evidenced by a high degree of data scattering between day-to-day river transects (Figs. S2c–d). We remark however a few extreme POC:TSM values at the highest salinity values in the rainy season. Spatial variation of POC:TSM along the river transect shows that these maxima were all found at high tide at the downstream sampling sites during the rainy season (Fig. S2d). A weak negative correlation was found between POC:PN and salinity (Fig. 7c). Similar to the spatial variation of POC, at high tide, POC:PN minima were also found toward the downstream end of the river transect in both seasons, while values gently increased before stabilizing towards the upstream sampling sites (Fig. S5g). Although POC and POC:PN did not show any clear spatial pattern for both seasons at low tides, which also agrees with high day-to-day variability between the corresponding individual river transects (Figs. S2e–f), both variables were higher at low than high tide

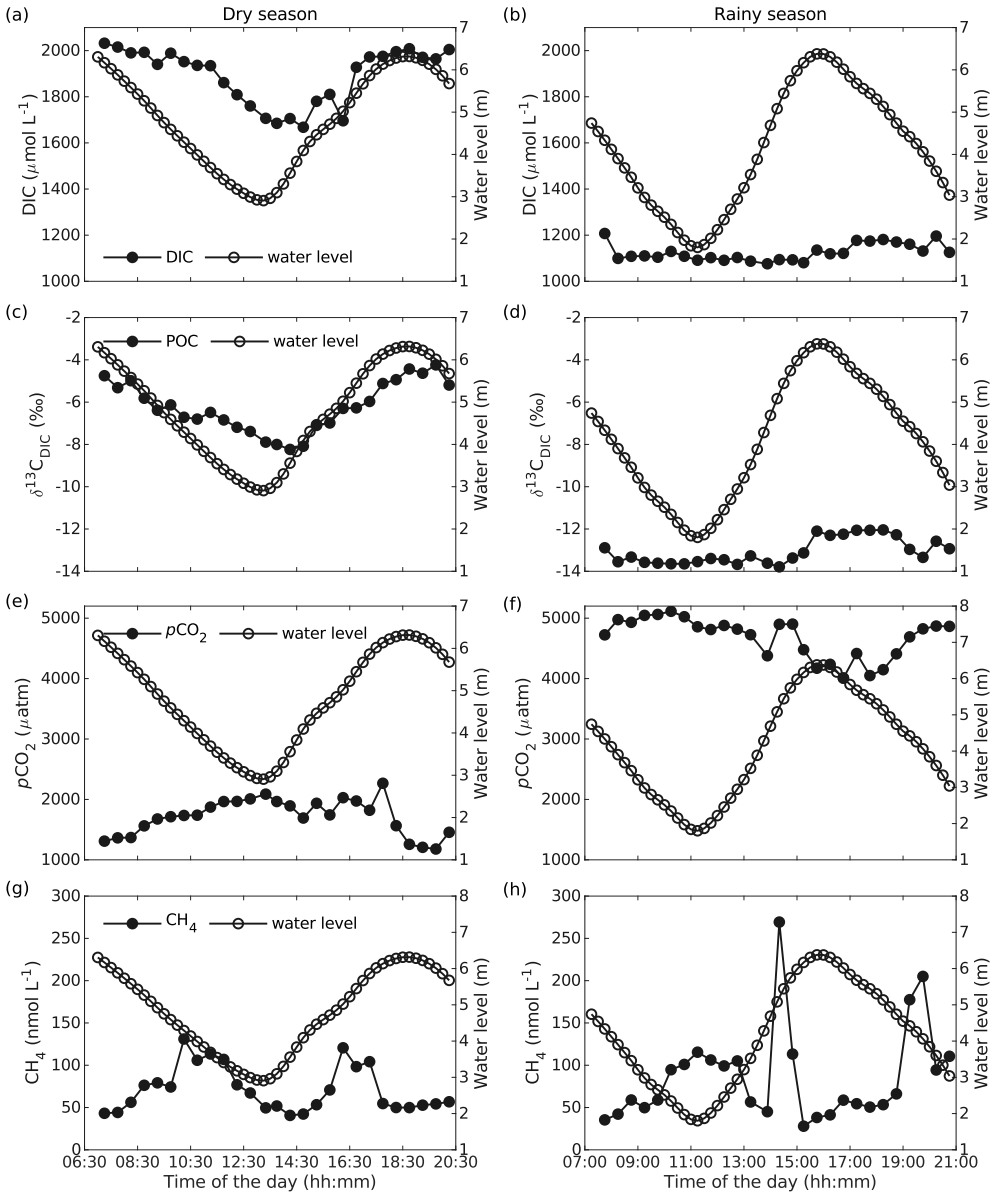

Fig. 5. Tidal variations of water levels and (a, b) DIC, (c, d) $\delta^{13}C_{DIC}$, (e, f) pCO_2 and (g, h) CH_4 in the dry (left panels) and rainy season (right panels). Data resulted from the sampling campaigns during semi-diurnal tidal cycles in the Guayas main channel in front of the village of Puerto Roma (see location in Fig. 1).

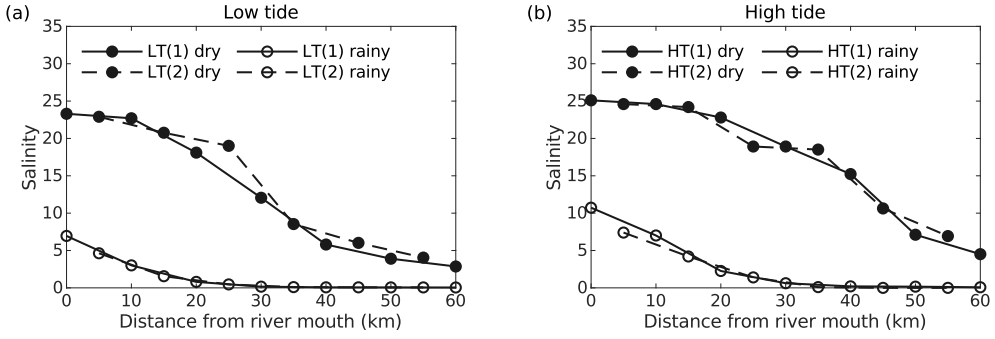

Fig. 6. Spatial variation of salinity along the Guayas river at (a) low tide (LT) and (b) high tides (HT) and during dry and rainy seasons. Two river cruises (1–2) were conducted per tidal stage and season on consecutive days to cover the full delta length at a 5 km resolution (see Methods).

in both seasons, with highest values observed during the dry season (Fig. S2).

$\delta^{13}C_{POC}$ on the other hand showed a significant and positive correlation with salinity ($\rho = 0.69$; $p < 0.05$; Fig. 7d). This corroborates with minimal changes between similar river transects, particularly during the dry season (Figs. S2g–h). Maxima were observed toward the

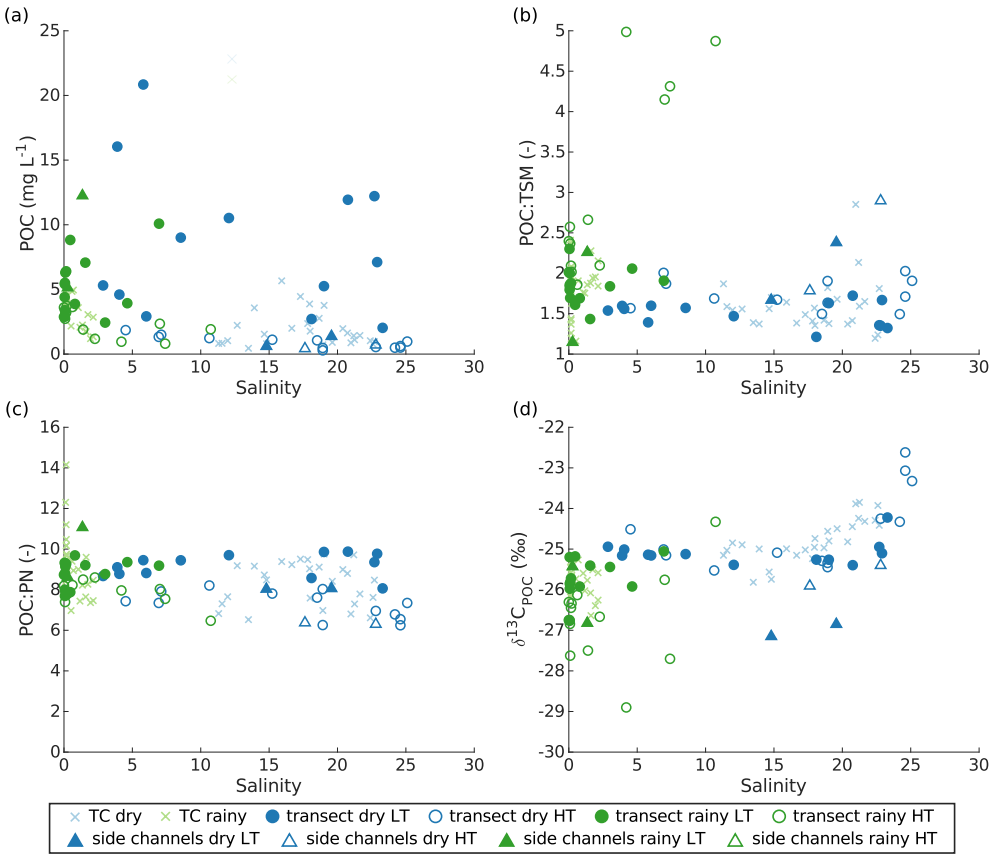

Fig. 7. Distribution of (a) POC, (b) POC:TSM, (c) POC:PN and (d) $\delta^{13}C_{POC}$ along the salinity gradient including all data collected along the river transects (circle symbols), at the side channels (triangle symbols), and at one site during semi-diurnal tidal cycles (TC; cross symbols) during the dry (blue tone symbols) and rainy (green tone symbols) seasons and at low tide (LT; filled symbols) and high tide (HT; empty symbols) tides. (For interpretation of the references to colour in this figure legend, the reader is referred to the Web version of this article.)

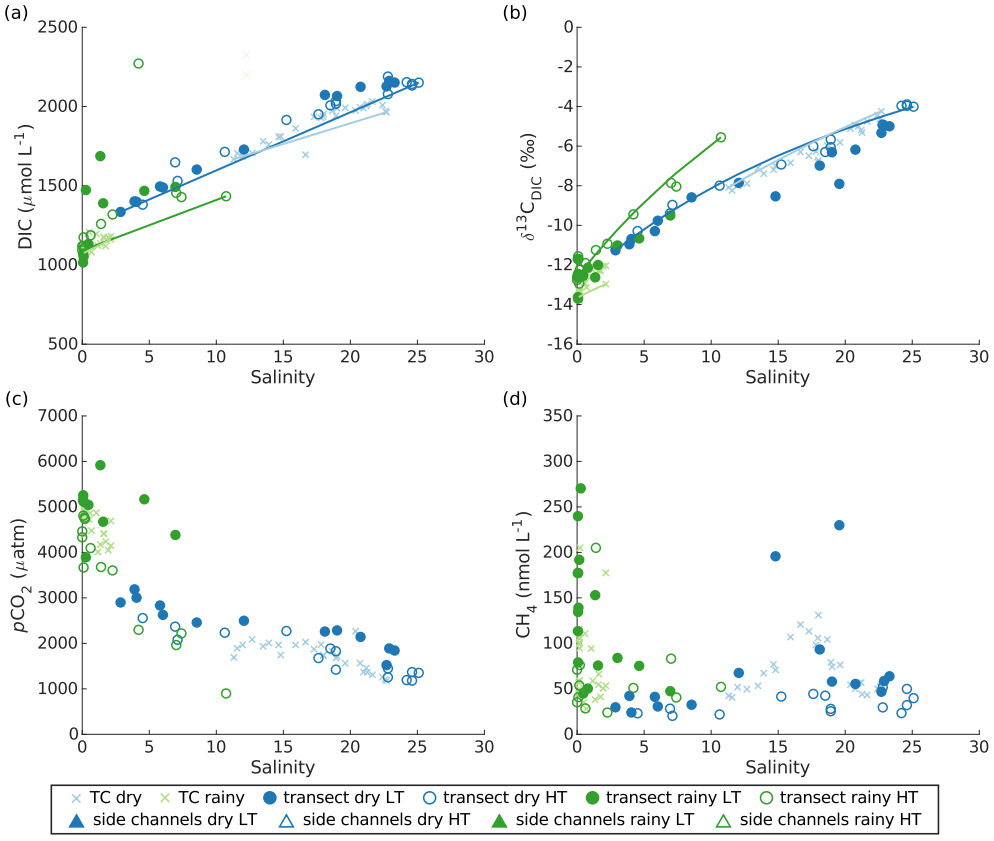

Fig. 8. Distribution of (a) DIC, (b) $\delta^{13}C_{DIC}$, (c) $pCOC_2$ and (d) CH_4 along the salinity gradient including all data collected along the river transects (circle symbols), at the side channels (triangle symbols), and at one site during semi-diurnal tidal cycles (TC; cross symbols) during the dry (blue tone symbols) and rainy (green tone symbols) seasons and at low tide (LT; filled symbols) and high tide (HT; empty symbols) tides. The conservative mixing predictions for DIC and $\delta^{13}C_{DIC}$ based on the river transect data and tidal cycle data, further differentiated per season are displayed. (For interpretation of the references to colour in this figure legend, the reader is referred to the Web version of this article.)

downstream end of the salinity gradient in both seasons. During the dry season, $\delta^{13}C_{POC}$ remained constant throughout most of the salinity gradient, apart from a sudden increase towards the marine end-member (Fig. S2g), whereas this increase appeared more gradual during the rainy season (Fig. S2h). In the dry season, $\delta^{13}C_{POC}$ values ranged from −27‰ to −22‰, while in the rainy season, values ranged from −29‰ to −24‰. When looking at the spatial variation of $\delta^{13}C_{POC}$ along the salinity gradient and river length, unlike POC and POC:PN, $\delta^{13}C_{POC}$ values were systematically higher at the downstream end of the river transect at high tide in both seasons (Figs. S2g–h and Fig. S5i), with an overall decrease upstream. Note that regardless the stage of the tide, $\delta^{13}C_{POC}$ values were lower during the rainy than dry season (Figs. S2g–h and Figs. S5i–j).

3.2.3. Dissolved inorganic carbon and methane dynamics

DIC and $\delta^{13}C_{DIC}$ both showed a strong positive correlation with salinity in both seasons ($\rho = 0.95$ and $\rho = 0.94$, respectively, both significant at $p < 0.05$ Fig. 8a–b). DIC concentrations ranged from 1300 to 2150 μmol L^{-1} in the dry season, and from 1000 to 2200 μmol L^{-1} in the rainy season. $\delta^{13}C_{DIC}$ was significantly higher in the dry than rainy season, with values varying from −11‰ to −4‰ and −14‰ to −5‰, respectively (Fig. 8b). Maxima and minima of DIC and $\delta^{13}C_{DIC}$ were found at the downstream and upstream ends of the sampled salinity gradient, respectively (see also Figs. S3a–d). This matches with the overall decrease in DIC and $\delta^{13}C_{DIC}$ found in the upstream direction in both seasons, for both low and high tides (Figs. S6a–b).

pCO_2 was negatively correlated to salinity in both seasons ($\rho = -0.90$; $p < 0.05$). pCO_2 showed a significant difference between dry and rainy seasons (Wilcoxon rank sum test: $Z = 8.11$, $p < 0.001$), with values ranging from 1000 to 3000 μatm in the dry season, and reaching almost 6000 μatm in the rainy season, revealing a significant seasonal shift (Fig. 8c). The river transect sampling showed that pCO_2 increased in the upstream direction in both seasons and both stages of the tide, from lowest values at the downstream end of the river transect to highest values at the upstream end (Figs. S6e–f). At low tide, pCO_2 ranged between 1500 and 3200 μatm in the dry season, and between 4400 and 5200 μatm in the rainy season (Figs. S3e–f and Fig. S6e). Comparatively, at high tide, pCO_2 ranged between 1200 and 2500 μatm in the dry season and between 900 and 4800 μatm in the rainy season (Fig. S6f). This reveals that tidal variations in pCO_2 were lower than seasonal variations. Unlike POC, pCO_2, $\delta^{13}C_{DIC}$ and DIC show minimal variations between individual river transects conducted at same tidal stage and season (Figs. S3a–f).

Comparatively, CH_4 showed a much weaker correlation with salinity ($\rho = -0.27$; $p < 0.05$). Minima and maxima occurred randomly in both seasons (Fig. 8d). CH_4 concentrations fluctuated around 20–230 nmol L^{-1} and 24–270 nmol L^{-1} in the dry and rainy seasons, respectively. In the dry season, maxima were observed in the side channels. Along the river transect, CH_4 overall gradually decreased in the upstream direction in the dry season, while in the rainy season, CH_4 varied more strongly and irregularly between sampling sites (Figs. S6g–h). High CH4 fluctuations were also observed between similar river transects (Figs. S3g–h).

4. Discussion

Despite carbon cycling in estuaries and deltas being recognized as a significant term in the global carbon budget, studies on the carbon biogeochemistry of tropical estuarine systems are still rather scarce, especially in the South American region. This contribution represents the first explorative survey of the spatio-temporal variations in different forms of carbon along the Guayas river delta (Ecuador). Our results indicate that tidal, seasonal and along-river variations in DIC concentration, $\delta^{13}C$ of DIC, and pCO_2 were strongly correlated with variations in salinity along these spatio-temporal scales, and so was the $\delta^{13}C$ of POC, albeit to a lower extent. In contrast, tidal, seasonal and along-river variations in POC and CH_4 concentrations are more independent from salinity variations and instead tend to follow variations in TSM, showing large variations over short time scales. Although it is difficult to identify the driving mechanisms behind these processes without further evidence, we can make some inferences on the source, processing and fate of these studied carbon forms, as well as estimates of the water-atmosphere exchange of CO_2 and CH_4 from this system, as we shall see thereafter.

4.1. Particulate organic carbon inputs, sources and processing

Tidal variation of POC concentrations (Fig. 4c–d), characterized by maxima at mid tides (i.e. when flood and ebb currents are typically highest) and minima at slack tides (i.e. when tidal currents are typically lowest), was consistent with observations from previous studies, as in a Brazilian estuarine system (Barboza et al., 2014) and a Tanzanian system (Bouillon et al., 2007c). Such patterns, combined with the strong correlation between POC and TSM, observed both during the tidal and river transect sampling (Fig. 4a–d and Figs. S4a–d), suggest that sediment resuspension during peak tidal flow velocities is an important driver of POC inputs in the water column.

Furthermore, our results point to the influence of the Guayas river discharge on POC inputs to the delta. We indeed observed seasonal differences in tidal variations of TSM and to a lower extent POC where, during periods of low water levels (early flood and later ebb stages), concentrations were lower in the dry season, but remained high during the rainy season (Fig. 4a–d). Similarly, our river transect sampling showed that POC concentrations at the most upstream sites at high tide was indeed higher in the rainy season. Mean POC concentrations over both tidal cycle and river transect sampling campaigns were also significantly higher during the rainy season (Table S1). Such trend can be explained by the fact that during the rainy season, the Guayas river contains higher suspended sediment loads at low tide, and its higher discharge and flow velocity may also allow to keep sediment in suspension, thus contributing to higher POC inputs in the water column. However, at low tide along the river transect, the POC concentration was higher in the dry season (Figs. S5c–d). The latter may be related to the large variations in TSM and POC concentrations that occur on short time scales (within diurnal and even semi-diurnal scales), as evidenced by notable differences between river transect sampling at same tidal stage and season; Figs. S2a–b), and the high fluctuations in the tidal cycle data (Fig. 4a–d). As we carried out our river transect sampling by cruising upstream following the low tidal wave as well as possible, it may be that we did not always sample exactly at low water slack, but that the upstream sites in the dry season (Fig. S5c) were sampled during a resuspension event shortly after low water slack, which could have resulted in fluctuations in the measured POC concentrations. The trend in POC concentrations against salinity is somewhat scattered, yet it shows an overall drecrease of POC concentration with increasing salinity (Fig. 7a), thus alluding indeed to an effect of the river discharge as a source of POC input to the delta.

The $\delta^{13}C_{POC}$ varied between −27‰ and −24‰ for most samples (Fig. 7c), which is similar to observations from a previous assessment of several tidal channels located within the Guayas river delta–Gulf of Guayaquil (Cifuentes et al., 1996). These $\delta^{13}C_{POC}$ values lie largely between typical values for marine algae (−18‰ to −22‰; Bardhan et al., 2015; Middelburg and Nieuwenhuize, 1998; Otero et al., 2000) and terrestrial, C_3 vegetation (−24‰ to −34‰; Bardhan et al., 2015; Smith and Epstein, 1971), thus indicating that sampled POC in the Guayas river consists of a mixture of marine and terrestrial material. This is confirmed by the values of POC:PN ratio which varied between 6 and 10, corresponding to values typical for highly degraded soil organic matter (8.1–12.9; Bala Krishna Prasad and Probst, 2005; Ittekkot and Zhang, 1989) but also overlapping with the upper range of marine phytoplankton (4.6–7.5; Bordovskiy, 1965; Müller, 1977). POC:TSM ratios mostly lie between 1 and 3, typical for the range of TSM found in world rivers (Ludwig et al., 1996a; Meybeck, 1982) and estuaries (Abril et al.,

2002). Overall, $\delta^{13}C_{POC}$ was higher with increasing salinity (Fig. 7d), which is consistent with slightly lower POC:PN ratios in the dry than rainy season (Fig. 7c). $\delta^{13}C_{POC}$ and POC:PN also showed a weak negative correlation (Fig. S5b). $\delta^{13}C_{POC}$ was also higher downstream (Figs. S5i–j) and POC:TSM ratios similarly showed maximum values downstream although only in the rainy season (Fig. S5h). All these observations suggest that there is a seasonal and spatial shift in POC sources from a relatively more phytoplankton dominated source in the dry season and downstream to a relatively more terrestrial source in the rainy season and upstream. Interestingly, $\delta^{13}C_{POC}$ did not show major differences between low and high tides when compiling both tidal cycle data and transect data, while the POC:PN ratio did, i.e. with higher POC:PN ratio at low tide (Table S1). This may indicate that resuspended carbon rich material remained in suspension at low tide, or that there was the presence of an inflow of carbon poor marine material at high tide.

4.2. Dissolved inorganic carbon inputs, sources and processing

Our observations showed that DIC increased with salinity (Fig. 8a), a trend that differs from observations in Indian estuarine systems (Bouillon et al., 2003), but agrees with observations in several other systems such as in the US Gulf coast (He and Xu, 2018) and Madagascar (Ralison et al., 2008). Contrary to these studies, DIC minima observed here were much higher (around 1000 μmol L^{-1} compared to < 500 μmol L^{-1}), which points to high bicarbonate (HCO_3^-) contents, possibly as a result of high weathering rates in the Guayas river basin encompassing the western Andean foothills. DIC maxima observed here (around 2200 μmol L^{-1}) were similar to oceanic values (1900–2500 μmol L^{-1}; Doi et al., 2015).

The $\delta^{13}C_{DIC}$ also showed a typical increasing trend with salinity (Fig. 8b), which suggests the mixing of freshwater coming from upstream, characterized by a more ^{13}C depleted signature, with marine water coming from downstream, characterized by the most ^{13}C enriched signatures (with values close to 0‰). This indicates a shift from DIC derived from weathering and degradation of terrestrial organic matter upstream to oceanic DIC downstream. The $\delta^{13}C_{DIC}$ of −4‰ measured at the downstream end of our river transect (at salinity equal to 25) nicely matches with observation from other studies (e.g. Bouillon et al., 2003), while the $\delta^{13}C_{DIC}$ measured at the upstream end of the river transect (~-14‰) showed more variability when compared with previous reported values (Guo et al., 2015; Ralison et al., 2008). The latter may be due to differences between estuarine systems in factors like vegetation type (C_3 vs. C_4; Bouillon et al., 2003; Smith and Epstein, 1971), land use and cover, and geology of the river catchment (Barth et al., 2003; Li et al., 2010; Probst et al., 1994).

Due to small deviations from conservative mixing along the salinity gradient, DIC and $\delta^{13}C_{DIC}$ did not behave conservatively (Fig. 8a–b). DIC and $\delta^{13}C_{DIC}$ measurements were indeed consistently higher and lower than expected along the salinity gradient, respectively, especially in the rainy season. These observations suggest inputs of relatively ^{13}C depleted DIC from mineralization along the salinity gradient (Borges et al., 2018; Bouillon et al., 2003; Saumik et al., 2015), which may include mangrove litter, as other potentially contributing processes (e.g. outgassing, primary production, and carbonate dissolution) would have resulted in more positive $\delta^{13}C_{DIC}$ values.

Tidal variation of DIC measurements did not suggest at first an influence of porewater seepage from adjacent mangrove forests during ebb tides. However, as we conducted our tidal cycle campaign in the main channel of the Guayas River delta (>2 km wide; see Fig. 1), such influence might have been masked due to the large water volume flowing through this channel and the comparatively low contribution of porewater seepage from adjacent mangrove forests. The lower $\delta^{13}C_{DIC}$ values measured in side channels (see Fig. 8b), might in fact indicate a porewater influence (although due to technical issues we did not have DIC concentration data for this particular day) or a higher contribution of DIC derived from the degradation of terrestrial material (Saumik et al., 2015). Measurements of DO and CH_4 (Fig. 8d) also indicate a higher relative porewater contribution at these particular stations at low tide (Bouillon et al., 2007b; Taillardat et al., 2018).

High pCO_2 measured in the Guayas river delta (1000–6000 μatm) indicates that this estuarine system, similar to many others (Borges and Abril, 2012), transports largely CO_2 oversaturated waters. pCO_2 depicts a decreasing relationship with salinity, with maxima and minima at the upstream and downstream end of the sampled river transect (Fig. 8c), respectively. Furthermore pCO_2 showed significantly negative correlations with $\%O_2$ and $\delta^{13}C_{DIC}$ (Fig. S7c). As such, high pCO_2 values, particularly observed upstream, correspond with $\%O_2$ undersaturation and low $\delta^{13}C_{DIC}$, therefore indicative of organic matter degradation, and a strongly heterotrophic system. Additionally, pCO_2 values were considerably higher in the rainy than dry season, which is likely explained by the drastic drop in salinity during the rainy season, as riverine CO_2 is typically high in riverine water in general (Cole et al., 2001), and more so in tropical rivers (Borges et al., 2015). Other studies have found that higher river discharge periods, as in the rainy season, are accompanied by a shift towards a more heterotrophic state due to the shorter water residence time preventing meaningful phytoplankton development (e.g. Borges et al., 2018). Estimates of residence time in the Guayas river range as short as 4 days during high river discharge conditions (i.e. 1600 m^3 s^{-1}; Arreaga Vargas, 2000), and lower $\%O_2$ observed in the rainy season point to a high rate of respiration in the water column. Yet, a lack of chlorophyll-*a* data prevent us from making robust conclusions on the presence of primary producers in the water column.

4.3. CH_4 inputs, sources and processing

Higher CH_4 concentrations were also observed in the rainy season, consistent with observations from other mangrove dominated estuaries in Australia (Rosentreter et al., 2018a), Vietnam (Borges and Abril, 2012), and India (Araujo et al., 2018). Previous studies have also shown that CH_4 concentrations typically decrease in the downstream direction in estuarine systems (Borges and Abril, 2012; Jeffrey et al., 2018; Middelburg et al., 2002), due to a series of processes, including CH_4 emission to the atmosphere (Araujo et al., 2018; Borges and Abril, 2012), microbial CH_4 oxidation (Borges and Abril, 2012; Knittel and Boetius, 2009) and mixing with marine water with a low CH_4 content (Borges et al., 2018; Rhee et al., 2009). Although we did observe an upstream increase in CH_4 during our low tide transect sampling in the rainy season, we did not observe it for the high tides or in the dry season, possibly due to a higher CH_4-poor seawater contribution in this system.

Tidal variations showed that CH_4 maxima and minima coincided with POC and TSM maxima and minima (compare Fig. 5 g-h against Fig. 4a–d), which may suggest that CH_4 was released from sediments during resuspension events at high tidal flow velocities. In addition, there were indications that CH_4-rich porewater seeping from the adjacent mangrove forests might have a notable influence on water column concentrations in certain areas or at certain times. For instance, at low tide in the rainy season there was a prolounged increase in CH_4 in the water column which quickly dropped once the tide started rising (Fig. 5h). More clearly still are the relative outliers of samples taken in the side channels, especially in the dry season (Fig. 8d). These observations, with high CH_4 levels, probably suggest a high relative contribution of porewater in the water column from the adjacent mangrove forest.

4.4. Estimations of CO_2 and CH_4 diffusive efflux to the atmosphere

Our estimations of CO_2 efflux, suggest that daily mean CO_2 efflux towards the atmosphere in the rainy season was significantly higher than in the dry season (Table 1), regardless of the gas transfer velocity parametrization values as proposed in Borges et al. (2004). This may be most likely due to the lower salinity and higher river discharge typical of

Table 1
Daily (per season and unit catchment area) and annual mean carbon diffusive fluxes for (a) CO_2, (b) CH_4, (c) POC and (d) DIC. CO_2 emissions are computed according to the Scheldt and Thames parametrization in Borges et al. (2004) for which two wind speed representative values are used. Similarly, CH_4 emissions are computed according to the parametrization by Raymond and Cole (2001).

(a)	Wind speed ($m\ s^{-1}$)	Dry season CO_2 efflux ($mmol\ m^{-2}\ day^{-1}$)	Rainy season CO_2 efflux ($mmol\ m^{-2}\ day^{-1}$)	Annual CO_2 efflux ($mol\ year^{-1}$)
Scheldt	0	46.1 ± 17.5	137.7 ± 32.1	29.8 ± 18.5
	2	129.7 ± 49.2	387.7 ± 90.2	84.0 ± 52.1
Thames	0	117.6 ± 44.6	351.4 ± 81.8	76.1 ± 47.3
	2	205.9 ± 78.0	615.2 ± 143.2	133.2 ± 82.7
(b)	Wind speed ($m\ s^{-1}$)	Dry season CH_4 efflux ($\mu mol\ m^{-2}\ day^{-1}$)	Rainy season CH_4 efflux ($\mu mol\ m^{-2}\ day^{-1}$)	Annual CH_4 efflux ($mmol\ year^{-1}$)
	0	24.9 ± 16.6	42.0 ± 28.5	11.7 ± 4.0
	2	45.3 ± 30.2	76.5 ± 51.9	21.3 ± 7.2
(c)		Dry season POC export rate ($mmol\ m^{-2}\ day^{-1}$)	Rainy season POC export rate ($mmol\ m^{-2}\ day^{-1}$)	Annual POC export rate ($Gmol\ year^{-1}$)
		0.36 ± 0.2	0.856 ± 0.3	9.4 ± 3.7
(d)		Dry season DIC export rate ($mmol\ m^{-2}\ day^{-1}$)	Rainy season DIC export rate ($mmol\ m^{-2}\ day^{-1}$)	Annual DIC export rate ($Gmol\ year^{-1}$)
		0.8 ± 0.6	2.7 ± 1.0	24.7 ± 9.7

the rainy season, which are factors influencing pCO_2 levels, as discussed previously. Our pCO_2 data that showed high levels of CO_2 oversaturation result in high estimates of annual mean CO_2 emission to the atmosphere from the Guayas river delta. These CO_2 emission estimates indeed largely exceed the mean (26 ± 21 mol m^{-2} yr^{-1}) and partly maxima (80 mol m^{-2} yr^{-1}) documented in a global review on greenhouse gases dynamics in estuarine systems (Borges and Abril, 2012). CH_4 efflux was also higher during the rainy than dry season, probably driven by the higher CH_4 concentration during the rainy season. Yet the daily mean CH_4 emissions we estimated (Table 1) were lower than most estuarine systems reported in the global review by Borges and Abril (2012) and the average of 124 estuarine sites compiled by Rosentreter et al. (2021). Further studies would be required to assess the factors contributing to these low CH_4 emissions.

4.5. Carbon export to the Gulf of Guayaquil

To the best of our knowledge, the export of various carbon forms from the Guayas river delta to the donwstream Gulf of Guayaquil and coastal waters has never been assessed. Here, we perform a tentative estimation of the carbon export based on available river discharge measurements at the freshwater end-member, assuming negligible changes in the carbon concentration and river discharge along the delta (see Methods). We found that the annual POC export rate in the Guayas river is likely comprised between 5.7 and 13.1 Gmol C yr^{-1} (i.e. 0.16 and 0.36 mol C m^{-2} yr^{-1} per unit catchment area). By comparison, our estimates of annual DIC export ranged between 15.0 and 34.4 Gmol C yr^{-1} (i.e. 0.42 and 0.98 mol C m^{-2} yr^{-1}). Such a significantly higher DIC export rate, as compared to POC export rate, has been also observed in various other mangrove dominated estuarine systems. Yearly riverine DIC export rates normalized by catchment area were in the same order of magnitude as those reported for several (sub-)tropical estuarine systems of similar size along the coast of Sumatra, Indonesia (Wit et al., 2018), the coast of India (Krishna et al., 2019) as well as one system in Cameroon (Brunet et al., 2009). These DIC export rates were even comparable to rates from larger (sub-)tropical estuaries (Cai et al., 2008) including the Pearl river estuary, China (Guo et al., 2008) and Yangtze river estuary, China (Wu et al., 2007). Daily DIC export rates per unit catchment area were however one to two order(s) of magnitude lower than those reported in tidal creeks in mangrove forests such as in Micronesia (Call et al., 2019), Australia (Maher et al., 2013; Sadat-Noori et al., 2016; Santos et al., 2019; Sippo et al., 2016), Vietnam (Taillardat et al., 2018), and compared to the global estimate of Bouillon et al. (2008). These lower rates may be explained by the fact that the latter studies measured DIC exports in tidal creeks dissecting mangrove forests and draining a much smaller area, thus representing a different geomorphic setting in which DIC export rates tend to be high (Bouillon et al., 2008).

5. Conclusions

This study presents an explorative survey of the carbon biogeochemistry in the Guayas river delta, Ecuador. In particular, the variability of different forms of carbon including POC, DIC and their stable isotope ratios, CO_2 and CH_4 were quantified across relevant spatio-temporal scales of interest in order to infer on the carbon sources, processing and fluxes across the system. Our data indicate significant tidal, seasonal and along-river variations of the concentrations and stable isotope composition of these particulate and dissolved carbon forms. These dynamics are driven by the transport and mixing of seawater and freshwater associated with biogeochemical processes along the salinity gradient, erosion of the catchment, river discharge and tidal hydrodynamics, and porewater exchange. We found high pCO_2 values associated with undersaturated $\%O_2$ levels, indicative of organic matter degration in the system and resulting in a high CO_2 efflux to the atmosphere. Our tentative estimates for carbon export from the Guayas river show a DIC export rate and especially POC export rate per unit catchment area far exceeding values reported for other tropical estuarine systems. A more detailed spatial sampling strategy accounting for the spatial complexity of such estuarine system combined with measurements of other carbon forms, e.g. DOC, and specific processes like primary production, and mineralization is however necessary for a comprehensive picture of the carbon biogeochemistry. Due to the overall data scarcity in tropical estuarine systems, particularly in the South American tropical Pacfic region, similar surveys are encouraged to improve estuarine carbon inventory in data scarce regions and reduce uncertainties in coastal zone carbon budgets.

CRediT authorship contribution statement

Jean-Philippe Belliard: Conceptualization, Data curation, Investigation, Methodology, Visualization, Writing – original draft, Writing – review & editing. **Simon Hernandez:** Conceptualization, Data curation, Formal analysis, Investigation, Methodology, Visualization, Writing – review & editing. **Stijn Temmerman:** Conceptualization, Funding acquisition, Methodology, Project administration, Supervision, Writing – review & editing. **Rey Harvey Suello:** Investigation, Writing – review & editing. **Luis E. Dominguez-Granda:** Conceptualization, Methodology, Resources, Writing – review & editing. **Andrea M. Rosado-Moncayo:** Investigation, Methodology, Writing – review & editing. **John A. Ramos-Veliz:** Investigation, Methodology, Writing – review & editing. **Rebeca N. Parra-Narera:** Investigation, Methodology, Writing – review & editing. **Karem P. Ramirez:** Investigation, Methodology, Writing – review & editing. **Gerard Govers:** Funding acquisition, Project administration, Supervision, Writing – review & editing. **Alberto V. Borges:** Resources, Supervision, Writing – review & editing. **Steven Bouillon:** Conceptualization, Funding acquisition, Methodology, Project

administration, Resources, Supervision, Writing – review & editing.

Declaration of competing interest

The authors declare that they have no known competing financial interests or personal relationships that could have appeared to influence the work reported in this paper.

Acknowledgements

This work was supported by the Research Foundation of Flanders, Belgium (FWO grant nr: G.0600.18N), as well as Vlaamse Interuniversitaire Raad - Universitaire Ontwikkelingssamenwerking (VLIR-UOS) and ActUA Prijs – University of Antwerp. We are very grateful to the fishermen of the Puerto Roma community, Guayas province, Ecuador for their transportation and logistic support in the field. Field work was granted by the Ecuadorian Ministry of Environment (MAE; research permit: 012-2018-IC-FLO/FAU-DPAG/MAE). A.V. Borges is a research director at the Fonds National de la Recherche Scientifique (Belgium). Finally, we thank Prof. Isaac Santos and two anonymous reviewers for their constructive reviews.

Appendix A. Supplementary data

Supplementary data to this article can be found online at https://doi.org/10.1016/j.ecss.2022.107766.

References

Abril, G., Nogueira, M., Etcheber, H., Cabeçadas, G., Lemaire, E., Brogueira, M.J., 2002. Behaviour of organic carbon in nine contrasting European estuaries. Estuar. Coast Shelf Sci. 54 (2), 241–262. https://doi.org/10.1006/ecss.2001.0844.

Alongi, D.M., 2014. Carbon cycling and storage in mangrove forests. Ann. Rev. Mar. Sci 6 (May), 195–219. https://doi.org/10.1146/annurev-marine-010213-135020.

Alongi, D.M., Mukhopadhyay, S.K., 2015. Contribution of mangroves to coastal carbon cycling in low latitude seas. Agric. For. Meteorol. 213, 266–272. https://doi.org/10.1016/j.agrformet.2014.10.005.

Araujo, J., Naqvi, S.W.A., Naik, H., Naik, R., 2018. Biogeochemistry of methane in a tropical monsoonal estuarine system along the west coast of India. Estuar. Coast Shelf Sci. 207, 435–443. https://doi.org/10.1016/j.ecss.2017.07.016.

Arreaga Vargas, P., 2000. Analysis del comportamiento de la salinidad (intrusion salina) en el sistema Río Guayas Canal de Jambeli como parte del cambio climatica. Acta Oceanográfico Del Pacifico 10 (1).

Atwood, T.B., Connolly, R.M., Almahasheer, H., Carnell, P.E., Duarte, C.M., Lewis, C.J.E., Irigoien, X., Kelleway, J.J., Lavery, P.S., Macreadie, P.I., Serrano, O., Sanders, C.J., Santos, I.R., Steven, A.D.L., Lovelock, C.E., 2017. Global patterns in mangrove soil carbon stocks and losses. Nat. Clim. Change 7 (7), 523–528. https://doi.org/10.1038/nclimate3326.

Bala Krishna Prasad, M., Probst, J.-L., 2005. Organic carbon transport and C/N ratio variations in a large tropical river: Godavari as a case study, India. Biogeochemistry 73 (3), 457–473. https://doi.org/10.1007/s10533-004-0879-2.

Bala Krishna Prasad, M., Ramanathan, A.L., 2009. Organic matter characterization in a tropical estuarine-mangrove ecosystem of India: preliminary assessment by using stable isotopes and lignin phenols. Estuar. Coast Shelf Sci. 84 (4), 617–624. https://doi.org/10.1016/j.ecss.2009.07.029.

Barboza, C.D.N., Paes, E.T., de Andrade Jandre, K., Marques, A.N., 2014. Concentrations and fluxes of nutrients and suspended organic matter in a tropical estuarine system: the Tinharé-Boipeba islands Archipelago (Baixo Sul Baiano, Brazil). J. Coast Res. 298, 1197–1209. https://doi.org/10.2112/jcoastres-d-12-00095.1.

Bardhan, P., Karapurkar, S.G., Shenoy, D.M., Kurian, S., Sarkar, A., Maya, M.V., Naik, H., Varik, S., Naqvi, S.W.A., 2015. Carbon and nitrogen isotopic composition of suspended particulate organic matter in Zuari Estuary, west coast of India. J. Mar. Syst. 141, 90–97. https://doi.org/10.1016/j.jmarsys.2014.07.009.

Barth, J.A.C., Cronin, A.A., Dunlop, J., Kalin, R.M., 2003. Influence of carbonates on the riverine carbon cycle in an anthropogenically dominated catchment basin: evidence from major elements and stable carbon isotopes in the Lagan River (N. Ireland). Chem. Geol. 200 (3), 203–216. https://doi.org/10.1016/S0009-2541(03)00193-1.

Bauer, J.E., Cai, W.J., Raymond, P.A., Bianchi, T.S., Hopkinson, C.S., Regnier, P.A.G., 2013. The changing carbon cycle of the coastal ocean. In: Nature, 504. Nature Publishing Group, pp. 61–70. https://doi.org/10.1038/nature12857, 7478.

Belliard, J.-P., Dominguez-Granda, L.E., Ramos-Veliz, J.A., Rosado-Moncayo, A.M., Nath, J., Govers, G., Gourgue, O., Temmerman, S., 2021. El Niño driven extreme sea levels in an Eastern Pacific tropical river delta: landward amplification and shift from oceanic to fluvial forcing. Global Planet. Change 203 (May), 103529.

Beusen, A.H.W., Dekkers, A.L.M., Bouwman, A.F., Ludwig, W., Harrison, J., 2005. Estimation of global river transport of sediments and associated particulate C, N, and P. Global Biogeochem. Cycles 19 (4). https://doi.org/10.1029/2005GB002453.

Borbor-Cordova, M.J., Boyer, E.W., Mcdowell, W.H., Hall, C.A., 2006. Nitrogen and phosphorus budgets for a tropical watershed impacted by agricultural land use: Guayas, Ecuador. Biogeochemistry 79 (1–2), 135–161. https://doi.org/10.1007/s10533-006-9009-7.

Bordovskiy, O.K., 1965. Sources of organic matter in marine basins. Mar. Geol. 3 (1), 5–31. https://doi.org/10.1016/0025-3227(65)90003-4.

Borges, A.V., 2005. Do we have enough pieces of the jigsaw to integrate CO2 fluxes in the coastal ocean? Estuaries 28 (1), 3–27. https://doi.org/10.1007/BF02732750.

Borges, A.V., Abril, G., 2012. Carbon dioxide and methane dynamics in estuaries. Treatise on Estuarine and Coastal Science 5. https://doi.org/10.1016/B978-0-12-374711-2.00504-0. Issue August 2018.

Borges, A.V., Abril, G., Bouillon, S., 2018. Carbon dynamics and CO2 and CH4 outgassing in the Mekong delta. Biogeosciences 15 (4), 1093–1114. https://doi.org/10.5194/bg-15-1093-2018.

Borges, A.V., Darchambeau, F., Teodoru, C.R., Marwick, T.R., Tamooh, F., Geeraert, N., Omengo, F.O., Guérin, F., Lambert, T., Morana, C., Okuku, E., Bouillon, S., 2015. Globally significant greenhouse-gas emissions from African inland waters. Nat. Geosci. 8 (8), 637–642. https://doi.org/10.1038/ngeo2486.

Borges, A.V., Delille, B., Schiettecatte, L.-S., Gazeau, F., Abril, G., Frankignoulle, M., 2004. Gas transfer velocities of CO2 in three European estuaries (Randers Fjord, Scheldt, and Thames). Limnol. Oceanogr. 49 (5), 1630–1641. https://doi.org/10.4319/lo.2004.49.5.1630.

Bouillon, S., Borges, A.V., Castañeda-Moya, E., Diele, K., Dittmar, T., Duke, N.C., Kristensen, E., Lee, S.Y., Marchand, C., Middelburg, J.J., Rivera-Monroy, V.H., Smith III, T.J., Twilley, R.R., 2008. Mangrove production and carbon sinks: a revision of global budget estimates. Global Biogeochem. Cycles 22 (2). https://doi.org/10.1029/2007GB003052.

Bouillon, S., Dehairs, F., Schiettecatte, L.-S., Borges, A.V., 2007b. Biogeochemistry of the Tana estuary and delta (northern Kenya). Limnol. Oceanogr. 52 (1), 46–59. https://doi.org/10.4319/lo.2007.52.1.0046.

Bouillon, S., Dehairs, F., Velimirov, B., Abril, G., Borges, A.V., 2007a. Dynamics of organic and inorganic carbon across contiguous mangrove and seagrass systems (Gazi Bay, Kenya). J. Geophys. Res.: Biogeosciences 112 (2). https://doi.org/10.1029/2006JG000325.

Bouillon, S., Frankignoulle, M., Dehairs, F., Velimirov, B., Eiler, A., Abril, G., Etcheber, H., Borges, A.V., 2003. Inorganic and organic carbon biogeochemistry in the Gautami Godavari estuary (Andhra Pradesh, India) during pre-monsoon: the local impact of extensive mangrove forests. Global Biogeochem. Cycles 17 (4). https://doi.org/10.1029/2002GB002026 n/a-n/a.

Bouillon, S., Middelburg, J.J., Dehairs, F., Borges, A.V., Abril, G., Flindt, M.R., Ulomi, S., Kristensen, E., 2007c. Importance of intertidal intertidal sediment processes and porewater exchange on the water column biogeochemistry in a pristine mangrove creek (Ras Dege, Tanzania). Biogeosciences 4 (3), 311–322. https://doi.org/10.5194/bg-4-311-2007.

Caffrey, J.M., 2004. Factors Controlling Net Ecosystem Metabolism in U . S. Estuaries 27 (1), 90–101.

Cai, W.-J., Guo, X., Chen, C.-T.A., Dai, M., Zhang, L., Zhai, W., Lohrenz, S.E., Yin, K., Harrison, P.J., Wang, Y., 2008. A comparative overview of weathering intensity and HCO3− flux in the world's major rivers with emphasis on the Changjiang, Huanghe, Zhujiang (Pearl) and Mississippi Rivers. Continent. Shelf Res. 28 (12), 1538–1549. https://doi.org/10.1016/j.csr.2007.10.014.

Call, M., Sanders, C.J., Macklin, P.A., Santos, I.R., Maher, D.T., 2019. Carbon outwelling and emissions from two contrasting mangrove creeks during the monsoon storm season in Palau, Micronesia. Estuar. Coast Shelf Sci. 218, 340–348. https://doi.org/10.1016/j.ecss.2019.01.002.

Cifuentes, L.A., Coffin, R.B., Solorzano, L., Cardenas, W., Espinoza, J., Twilley, R.R., 1996. Isotopic and elemental variations of carbon and nitrogen in a mangrove estuary. Estuar. Coast Shelf Sci. 43 (6), 781–800. https://doi.org/10.1006/ecss.1996.0103.

Cloern, J.E., Foster, S.Q., Kleckner, A.E., 2014. Phytoplankton primary production in the world's estuarine-coastal ecosystems. Biogeosciences 11 (9), 2477–2501. https://doi.org/10.5194/bg-11-2477-2014.

Cole, J.J., Cole, J.J., Caraco, N.F., Caraco, N.F., 2001. Carbon in catchments: connecting terrestrial carbon losses with aquatic metabolism. Mar. Freshw. Res. 52 (1), 101–110. https://doi.org/10.1071/MF00084.

Cole, J.J., Prairie, Y.T., Caraco, N.F., McDowell, W.H., Tranvik, L.J., Striegl, R.G., Duarte, C.M., Kortelainen, P., Downing, J.A., Middelburg, J.J., Melack, J., 2007. Plumbing the global carbon cycle: integrating inland waters into the terrestrial carbon budget. Ecosystems 10 (1), 171–184. https://doi.org/10.1007/s10021-006-9013-8.

Couto, T., Duarte, B., Caçador, I., Baeta, A., Marques, J.C., 2013. Salt marsh plants carbon storage in a temperate Atlantic estuary illustrated by a stable isotopic analysis based approach. Ecol. Indicat. 32, 305–311. https://doi.org/10.1016/j.ecolind.2013.04.004.

Damanik-Ambarita, M.N., Boets, P., Nguyen Thi, H.T., Forio, M.A.E., Everaert, G., Lock, K., Musonge, P.L.S., Suhareva, N., Bennetsen, E., Gobeyn, S., Ho, T.L., Dominguez-Granda, L., Goethals, P.L.M., 2018. Impact assessment of local land use on ecological water quality of the Guayas river basin (Ecuador). Ecol. Inf. 48, 226–237. https://doi.org/10.1016/j.ecoinf.2018.08.009.

Deknock, A., De Troyer, N., Houbraken, M., Dominguez-Granda, L., Nolivos, I., Van Echelpoel, W., Forio, M.A.E., Spanoghe, P., Goethals, P.L.M., 2019. Distribution of agricultural pesticides in the freshwater environment of the Guayas river basin (Ecuador). Sci. Total Environ. 646, 996–1008. https://doi.org/10.1016/j.scitotenv.2018.07.185.

Doi, T., Osafune, S., Sugiura, N., Kouketsu, S., Murata, A., Masuda, S., Toyoda, T., 2015. Multidecadal change in the dissolved inorganic carbon in a long-term ocean state

estimation. J. Adv. Model. Earth Syst. 7 (4), 1885–1900. https://doi.org/10.1002/2015MS000462.
Donato, D.C., Kauffman, J.B., Murdiyarso, D., Kurnianto, S., Stidham, M., Kanninen, M., 2011. Mangroves among the most carbon-rich forests in the tropics. Nat. Geosci. 4 (5), 293–297. https://doi.org/10.1038/ngeo1123.
Gattuso, J.-P., Frankignoulle, M., Wollast, R., 1998. Carbon and carbonate metabolism IN coastal aquatic ecosystems. Annu. Rev. Ecol. Systemat. 29 (1), 405–434. https://doi.org/10.1146/annurev.ecolsys.29.1.405.
Guo, W., Ye, F., Xu, S., Jia, G., 2015. Seasonal variation in sources and processing of particulate organic carbon in the Pearl River estuary, South China. Estuar. Coast Shelf Sci. 167, 540–548. https://doi.org/10.1016/j.ecss.2015.11.004.
Guo, X., Cai, W.-J., Zhai, W., Dai, M., Wang, Y., Chen, B., 2008. Seasonal variations in the inorganic carbon system in the Pearl River (Zhujiang) estuary. Continent. Shelf Res. 28 (12), 1424–1434. https://doi.org/10.1016/j.csr.2007.07.011.
Hamlington, B.D., Cheon, S.H., Thompson, P.R., Merrifield, M.A., Nerem, R.S., Leben, R. R., Kim, K.Y., 2016. An ongoing shift in Pacific Ocean sea level. J. Geophys. Res.: Oceans 121 (7), 5084–5097. https://doi.org/10.1002/2016JC011815.
He, S., Xu, Y.J., 2018. Freshwater-saltwater mixing effects on dissolved carbon and CO2 outgassing of a coastal river entering the northern Gulf of Mexico. Estuar. Coast 41 (3), 734–750. https://doi.org/10.1007/s12237-017-0320-4.
Hoffman, J.C., Bronk, D.A., 2006. Interannual variation in stable carbon and nitrogen isotope biogeochemistry of the Mattaponi River, Virginia. Limnol. Oceanogr. 51 (5), 2319–2332. https://doi.org/10.4319/lo.2006.51.5.2319.
Huang, T.-H., Fu, Y.-H., Pan, P.-Y., Chen, C.-T.A., 2012. Fluvial carbon fluxes in tropical rivers. Curr. Opin. Environ. Sustain. 4 (2), 162–169. https://doi.org/10.1016/j.cosust.2012.02.004.
ICEX, 2019. In: *Estudios de mercados. El mercado de pesca y acuacultura en Ecuador 2019* (ICEX Espana Exportacion e Inversiones.
INOCAR, 2019. Precipiation en Guayaquil. https://www.inocar.mil.ec/web/index.php/precipitacion-en-guayaquil.
Ittekkot, V., Zhang, S., 1989. Pattern of particulate nitrogen transport in world rivers. Global Biogeochem. Cycles 3 (4), 383–391. https://doi.org/10.1029/GB003i004p00383.
Jeffrey, L.C., Maher, D.T., Santos, I.R., Call, M., Reading, M.J., Holloway, C., Tait, D.R., 2018. The spatial and temporal drivers of pCO2, pCH4 and gas transfer velocity within a subtropical estuary. Estuar. Coast Shelf Sci. 208, 83–95. https://doi.org/10.1016/j.ecss.2018.04.022.
Knittel, K., Boetius, A., 2009. Anaerobic Oxidation of Methane: Progress with an Unknown Process, vol. 63, pp. 311–334. https://doi.org/10.1146/annurev.micro.61.080706.093130.
Krishna, M.S., Viswanadham, R., Prasad, M.H.K., Kumari, V.R., Sarma, V.V.S.S., 2019. Export fluxes of dissolved inorganic carbon to the northern Indian Ocean from the Indian monsoonal rivers. Biogeosciences 16 (2), 505–519. https://doi.org/10.5194/bg-16-505-2019.
Lewis, E.R., Wallace, D.W.R., 1998. Program Developed for CO2 System Calculations. https://doi.org/10.15485/1464255.
Li, M., Peng, C., Wang, M., Xue, W., Zhang, K., Wang, K., Shi, G., Zhu, Q., 2017. The carbon flux of global rivers: a re-evaluation of amount and spatial patterns. Ecol. Indicat. 80, 40–51. https://doi.org/10.1016/J.ECOLIND.2017.04.049.
Li, S.-L., Liu, C.-Q., Li, J., Lang, Y.-C., Ding, H., Li, L., 2010. Geochemistry of dissolved inorganic carbon and carbonate weathering in a small typical karstic catchment of Southwest China: isotopic and chemical constraints. Chem. Geol. 277 (3), 301–309. https://doi.org/10.1016/j.chemgeo.2010.08.013.
Ludwig, W., Probst, J.-L., Kempe, S., 1996a. Predicting the oceanic input of organic carbon by continental erosion. Global Biogeochem. Cycles 10 (1), 23–41. https://doi.org/10.1029/95GB02925.
Ludwig, W., Suchet, P.A., Probst, J.-L., 1996b. River discharges of carbon to the world's oceans: determining local inputs of alkalinity and of dissolved and particulate organic carbon. In: Sciences de La Terre et Des Planètes (Comptes Rendus de l'Académie Des Sciences), vol. 323, pp. 1007–1014. https://oatao.univ-toulouse.fr/3498/.
Maher, D.T., Call, M., Santos, I.R., Sanders, C.J., 2018. Beyond burial: lateral exchange is a significant atmospheric carbon sink in mangrove forests. Biol. Lett. 14 (7) https://doi.org/10.1098/rsbl.2018.0200.
Maher, D.T., Santos, I.R., Golsby-Smith, L., Gleeson, J., Eyre, B.D., 2013. Groundwater-derived dissolved inorganic and organic carbon exports from a mangrove tidal creek: the missing mangrove carbon sink? Limnol. Oceanogr. 58 (2), 475–488. https://doi.org/10.4319/lo.2013.58.2.0475.
Meybeck, M., 1982. Carbon, nitrogen, and phosphorus transport by world rivers. Am. J. Sci. 282 (4), 401. https://doi.org/10.2475/ajs.282.4.401. LP – 450.
Middelburg, J.J., Nieuwenhuize, J., 1998. Carbon and nitrogen stable isotopes in suspended matter and sediments from the Schelde Estuary. Mar. Chem. 60 (3–4), 217–225. https://doi.org/10.1016/S0304-4203(97)00104-7.
Middelburg, J.J., Nieuwenhuize, J., Iversen, N., Høgh, N., de Wilde, H., Helder, W., Seifert, R., Christof, O., 2002. Methane distribution in European tidal estuaries. Biogeochemistry 59 (1), 95–119. https://doi.org/10.1023/A:1015515130419.
Mook, W.G., Tan, T.C., 1991. Stable carbon isotopes in rivers and estuaries. In: Degens, E. T., Al, E. (Eds.), Biogeochemistry of Major World Rivers. John Wiley, pp. 245–264.
Mouw, C.B., Barnett, A., McKinley, G.A., Gloege, L., Pilcher, D., 2016. Global ocean particulate organic carbon flux merged with satellite parameters. Earth Syst. Sci. Data 8 (2), 531–541. https://doi.org/10.5194/essd-8-531-2016.
Müller, P.J., 1977. CN ratios in Pacific deep-sea sediments: effect of inorganic ammonium and organic nitrogen compounds sorbed by clays. Geochem. Cosmochim. Acta 41 (6), 765–776. https://doi.org/10.1016/0016-7037(77)90047-3.
Otero, E., Culp, R., Noakes, J.E., Hodson, R.E., 2000. Allocation of particulate organic carbon from different sources in two contrasting estuaries of southeastern U.S.A. Limnol. Oceanogr. 45 (8), 1753–1763. https://doi.org/10.4319/lo.2000.45.8.1753.
Ouyang, X., Lee, S.Y., 2020. Improved estimates on global carbon stock and carbon pools in tidal wetlands. Nat. Commun. 11 (1) https://doi.org/10.1038/s41467-019-14120-2.
Probst, J.-L., Mortatti, J., Tardy, Y., 1994. Carbon river fluxes and weathering CO2 consumption in the Congo and Amazon river basins. Appl. Geochem. 9 (1), 1–13. https://doi.org/10.1016/0883-2927(94)90047-7.
Ralison, O.H., Borges, A.V., Dehairs, F., Middelburg, J.J., Bouillon, S., 2008. Carbon biogeochemistry of the Betsiboka estuary (north-western Madagascar). Org. Geochem. 39 (12), 1649–1658. https://doi.org/10.1016/j.orggeochem.2008.01.010.
Raymond, P.A., Cole, J.J., 2001. Gas Exchange in Rivers and Estuaries: Choosing a Gas Transfer Velocity. Estuaries 24 (2), 312–317. https://doi.org/10.2307/1352954.
Regnier, P.A.G., Friedlingstein, P., Ciais, P., Mackenzie, F.T., Gruber, N., Janssens, I.A., Laruelle, G.G., Lauerwald, R., Luyssaert, S., Andersson, A.J., Arndt, S., Arnosti, C., Borges, A.V., Dale, A.W., Gallego-Sala, A., Goddéris, Y., Goossens, N., Hartmann, J., Heinze, C., Thullner, M., 2013. Anthropogenic perturbation of the carbon fluxes from land to ocean. Nat. Geosci. 6 (8), 597–607. https://doi.org/10.1038/ngeo1830.
Rhee, T.S., Kettle, A.J., Andreae, M.O., 2009. Methane and nitrous oxide emissions from the ocean: A reassessment using basin-wide observations in the Atlantic. J. Geophys. Res. Atmos. 114 (D12), 12304 https://doi.org/10.1029/2008JD011662.
Rosentreter, J.A., Borges, A.V., Deemer, B.R., Holgerson, M.A., Liu, S., Song, C., Melack, J., Raymond, P.A., Duarte, C.M., Allen, G.H., Olefeldt, D., Poulter, B., Battin, T.I., Eyre, B.D., 2021. Half of global methane emissions come from highly variable aquatic ecosystem sources. Nat. Geosci. 14 (4), 225–230. https://doi.org/10.1038/s41561-021-00715-2.
Rosentreter, J.A., Maher, D.T., Erler, D.V., Murray, R.H., Eyre, B.D., 2018a. Methane emissions partially offset "blue carbon" burial in mangroves. Sci. Adv. 4 (6) https://doi.org/10.1126/sciadv.aao4985.
Rosentreter, J.A., Maher, D.T., Erler, D.V., Murray, R.H., Eyre, B.D., 2018b. Seasonal and temporal CO2 dynamics in three tropical mangrove creeks – A revision of global mangrove CO2 emissions. Geochem. Cosmochim. Acta 222 (February), 729–745. https://doi.org/10.1016/j.gca.2017.11.026.
Rovai, A.S., Twilley, R.R., Castañeda-Moya, E., Riul, P., Cifuentes-Jara, M., Manrow-Villalobos, M., Horta, P.A., Simonassi, J.C., Fonseca, A.L., Pagliosa, P.R., 2018. Global controls on carbon storage in mangrove soils. Nat. Clim. Change 8 (6), 534–538. https://doi.org/10.1038/s41558-018-0162-5.
Sadat-Noori, M., Maher, D.T., Santos, I.R., 2016. Groundwater Discharge as a Source of Dissolved Carbon and Greenhouse Gases in a Subtropical Estuary. Estuar. Coast 39 (3), 639–656. https://doi.org/10.1007/s12237-015-0042-4.
Santos, I.R., Maher, D.T., Larkin, R., Webb, J.R., Sanders, C.J., 2019. Carbon outwelling and outgassing vs. burial in an estuarine tidal creek surrounded by mangrove and saltmarsh wetlands. Limnol. Oceanogr. 64 (3), 996–1013. https://doi.org/10.1002/lno.11090.
Saumik, S., Dalai, T.K., Pattanaik, J.K., Rai, S.K., Mazumdar, A., 2015. Dissolved inorganic carbon (DIC) and its δ13C in the Ganga (Hooghly) River estuary, India: Evidence of DIC generation via organic carbon degradation and carbonate dissolution. Geochem. Cosmochim. Acta 165, 226–248. https://doi.org/10.1016/j.gca.2015.05.040.
Sippo, J.Z., Maher, D.T., Tait, D.R., Holloway, C., Santos, I.R., 2016. Are mangroves drivers or buffers of coastal acidification? Insights from alkalinity and dissolved inorganic carbon export estimates across a latitudinal transect. Global Biogeochem. Cycles 30, 753–766. https://doi.org/10.1002/2015GB005324.
Smith, B.N., Epstein, S., 1971. Two Categories of 13C/12C Ratios for Higher Plants. Plant Physiol. 47 (3), 380. https://doi.org/10.1104/pp.47.3.380. LP – 384.
Syvitski, J.P.M., Vörösmarty, C.J., Kettner, A.J., Green, P., 2005. Impact of Humans on the Flux of Terrestrial Sediment to the Global Coastal Ocean. https://doi.org/10.1126/science.1109454.
Taillardat, P., Willemsen, P.W.J.M., Marchand, C., Friess, D.A., Widory, D., Baudron, P., Truong, V.V., Nguyễn, T.N., Ziegler, A.D., 2018. Assessing the contribution of porewater discharge in carbon export and CO2 evasion in a mangrove tidal creek (Can Gio, Vietnam). J. Hydrol. 563, 303–318. https://doi.org/10.1016/j.jhydrol.2018.05.042.
Tue, N.T., Quy, T.D., Hamaoka, H., Nhuan, M.T., Omori, K., 2012. Sources and Exchange of Particulate Organic Matter in an Estuarine Mangrove Ecosystem of Xuan Thuy National Park, Vietnam. Estuar. Coast 35 (4), 1060–1068. https://doi.org/10.1007/s12237-012-9487-x.
Twilley, R.R., Cardenas, W., Rivera-Monroy, V.H., Espinoza, J., Suescum, R., Armijos, M. M., Solorzano, L., 2001. The Gulf of Guayaquil and the Guayas River Estuary Ecuador. In: Coastal Marine Ecosystems of Latin America.
Twilley, R.R., Pozo, M., Garcia, V.H., Rivera-Monroy, V.H., Zambrano, R., Bodero, A., 1997. Litter dynamics in riverine mangrove forests in the Guayas River estuary, Ecuador. Oecologia 111 (1), 109–122. https://doi.org/10.1007/s004420050214.
Twilley, R.R., Gottfried, R., Rivera-Monroy, V.H., Zhang, W., Montaño Armijos, M., Bodero, A., Gottfried, R.R., Zang, W., Armijos, M.M., 1998. An approach and preliminary model of integrating ecological and economic constraints of environmental quality in the Guayas River estuary, Ecuador. Environ. Sci. Pol. 1 (4), 271–288. https://doi.org/10.1016/S1462-9011(98)00012-4.
Vitousek, S., Barnard, P.L., Fletcher, C.H., Frazer, N., Erikson, L., Storlazzi, C.D., 2017. Doubling of coastal flooding frequency within decades due to sea-level rise. Sci. Rep. 7 (1), 1–9. https://doi.org/10.1038/s41598-017-01362-7.
Wit, F., Rixen, T., Baum, A., Pranowo, W.S., Hutahaean, A.A., 2018. The Invisible Carbon Footprint as a hidden impact of peatland degradation inducing marine carbonate

dissolution in Sumatra, Indonesia. Sci. Rep. 8 (1), 17403. https://doi.org/10.1038/s41598-018-35769-7.

Wu, Y., Zhang, J., Liu, S.M., Zhang, Z.F., Yao, Q.Z., Hong, G.H., Cooper, L., 2007. Sources and distribution of carbon within the Yangtze River system. Estuar. Coast Shelf Sci. 71 (1), 13–25. https://doi.org/10.1016/j.ecss.2006.08.016.

Yamamoto, S., Alcauskas, J.B., Crozier, T.E., 1976. Solubility of methane in distilled water and seawater. J. Chem. Eng. Data 21 (1), 78–80. https://doi.org/10.1021/je60068a029.

Zapata, C., Puente, A., García, A., García-Alba, J., Espinoza, J., 2019. The Use of Hydrodynamic Models in the Determination of the Chart Datum Shape in a Tropical Estuary. Water 11 (5), 902. https://doi.org/10.3390/W11050902.